
ARTEMIS: A NEURO-SYMBOLIC FRAMEWORK FOR ECONOMICALLY CONSTRAINED MARKET DYNAMICS

Rahul D Ray

Department of Electronics and Electrical Engineering
BITS Pilani, Hyderabad Campus
f20242213@hyderabad.bits-pilani.ac.in

ABSTRACT

Deep learning models in quantitative finance often operate as black boxes, lacking interpretability and failing to incorporate fundamental economic principles such as no arbitrage constraints. This paper introduces ARTEMIS (Arbitrage free Representation Through Economic Models & Interpretable Symbolics), a novel neuro symbolic framework that combines a continuous time encoder based on a Laplace Neural Operator, a neural stochastic differential equation regularised by physics informed losses, and a differentiable symbolic bottleneck that distills interpretable trading rules. The model enforces economic plausibility through two novel regularisation terms: a Feynman Kac PDE residual that penalises violations of local no arbitrage conditions, and a market price of risk penalty that bounds the instantaneous Sharpe ratio to realistic values. We evaluate ARTEMIS against six strong baselines including LSTM, Transformer, NS Transformer, Informer, Chronos 2, and XGBoost on four diverse datasets: Jane Street (anonymised market data) Desai et al. [2024], OptiverMeyer et al. [2021] (limit order book volatility prediction), Time IMM (environmental temperature forecasting) Chang et al. [2025], and DSLOB (a synthetic crash regime). Results demonstrate that ARTEMIS achieves state of the art directional accuracy, outperforming all baselines on DSLOB (64.96%) and Time IMM (96.0%), while remaining competitive on point accuracy metrics. A comprehensive ablation study on DSLOB confirms that each component contributes to this directional advantage: removing the PDE loss reduces directional accuracy from 64.89% to 50.32%, and removing both physics losses collapses it to 41.77%, worse than random. The underperformance on OptiverMeyer et al. [2021] is attributed to its long sequence length, volatility focused target, and limited feature set, highlighting important boundary conditions. By providing interpretable, economically grounded predictions without sacrificing performance, ARTEMIS bridges the gap between deep learning’s predictive power and the transparency demanded in quantitative finance, opening new avenues for trustworthy AI in high stakes financial applications.

1 Introduction

The application of deep learning to financial time series prediction has witnessed explosive growth over the past decade, driven by the increasing availability of high-frequency market data and the remarkable success of neural networks in capturing complex temporal patterns. From return forecasting and volatility prediction to algorithmic trading and risk management, deep learning models have demonstrated superior performance compared to traditional econometric approaches such as ARIMA and GARCH [Rundo et al., 2019, Ndikum, 2020]. Recent comprehensive surveys [Chen et al., 2024, Zhang et al., 2024, Giantsidi and Tarantola, 2025] document the rapid evolution of architectures from standalone models like Long Short-Term Memory (LSTM) networks and Convolutional Neural Networks (CNNs) to sophisticated hybrid systems that combine multiple techniques. However, despite these advances, the adoption of deep learning in high-stakes financial applications remains hampered by three fundamental challenges that the literature has consistently identified but not yet fully resolved.

The first and most widely recognised challenge is the lack of interpretability. As financial institutions operate under strict regulatory oversight, the opacity of deep learning models, often described as black boxes, creates significant legal, ethical, and operational risks [Rane et al., 2023, Hoang et al., 2026]. Stakeholders, including regulators

and risk managers, require transparent explanations for model decisions, particularly when those decisions involve substantial capital allocation or have the potential to impact market stability [Mathew et al., 2025]. While explainable artificial intelligence (XAI) techniques such as SHAP and LIME have been proposed to provide post-hoc explanations [Sokolovsky et al., 2023, Basha et al., 2025], these methods offer only approximate insights and do not address the underlying opacity of the model architecture itself. Moreover, they introduce an inherent trade-off between predictive accuracy and interpretability, where simpler, more transparent models often sacrifice the very complexity that enables superior performance [Rane et al., 2023, Mathew et al., 2025]. This tension between accuracy and transparency remains a central obstacle to deploying deep learning in production trading systems.

The second challenge concerns the integration of economic principles into data-driven models. Traditional financial models are built upon foundational theories such as the absence of arbitrage, which ensures that asset prices cannot be risklessly exploited for profit. Yet most deep learning approaches are trained purely on historical data, learning correlations without any regard for these economic constraints [Mashrur et al., 2020, Sahu et al., 2023]. As a consequence, they can discover spurious patterns that lead to implausible predictions, particularly when market conditions deviate from the training distribution [Suarez-Cetrulo et al., 2023, Hasan et al., 2023]. Recent work has begun to address this gap through physics-informed neural networks (PINNs), which embed governing equations into the loss function to enforce consistency with physical or financial laws. Pioneering studies have applied PINNs to option pricing models, including the Black-Scholes equation and the Heston model [Bai et al., 2022, Hainaut and Casas, 2024, Nuugulu et al., 2025], demonstrating improved accuracy and stability. Extensions have tackled jump-diffusion models with liquidity costs [Kartik and Shah, 2025] and fully nonlinear PDEs relevant to portfolio optimisation [Lefebvre et al., 2023]. However, these applications have focused primarily on solving known pricing equations rather than learning latent dynamics from data while simultaneously enforcing economic constraints. The synthesis of data-driven learning with physics-informed regularisation for forecasting tasks remains largely unexplored.

The third challenge relates to the continuous-time nature of financial markets and the non-stationarity of financial time series. Traditional discrete-time models struggle to process irregularly sampled, high-frequency data without interpolation, which can distort underlying dynamics [Han et al., 2024, Wang et al., 2025]. Moreover, market regimes shift over time, and models that perform well during stable periods often fail catastrophically during crises [Suarez-Cetrulo et al., 2023, Hasan et al., 2023]. Neural stochastic differential equations (neural SDEs) offer a promising continuous-time framework that can naturally accommodate irregular observations and capture uncertainty through stochastic dynamics [Wang et al., 2025]. Similarly, advances in handling non-stationarity, such as the Non-stationary Transformer [Zhang et al., 2024], have improved robustness to distribution shifts. Yet these approaches remain disconnected from the interpretability and economic constraint challenges described above.

In this paper, we introduce ARTEMIS (Arbitrage-free Representation Through Economic Models & Interpretable Symbolics), a novel neuro-symbolic framework that addresses all three challenges within a unified architecture. ARTEMIS makes the following key contributions:

- **Continuous-time encoding via Laplace Neural Operator.** Unlike standard recurrent or transformer models that require regularly sampled inputs, our encoder operates directly on irregularly spaced observations, preserving the true temporal structure of limit order book updates and trade reports without interpolation [Wang et al., 2025, Han et al., 2024].
- **Economics-informed latent dynamics through neural SDEs with physics-constrained regularisation.** We introduce two novel loss terms derived from the Fundamental Theorem of Asset Pricing: a Feynman-Kac PDE residual that enforces local no-arbitrage conditions in the latent space, and a market price of risk penalty that bounds the instantaneous Sharpe ratio to realistic values. While previous work has applied PINNs to pricing equations [Bai et al., 2022, Hainaut and Casas, 2024, Nuugulu et al., 2025, Kartik and Shah, 2025] and neural SDEs to continuous-time modelling [Wang et al., 2025], our work is the first to embed such economic constraints directly into the learning of latent dynamics for forecasting.
- **Differentiable symbolic bottleneck for interpretability.** Rather than relying on post-hoc explanations [Sokolovsky et al., 2023, Basha et al., 2025], we design a layer that distills the latent dynamics into closed-form, interpretable expressions through differentiable symbolic regression. This provides inherent transparency while maintaining end-to-end trainability, offering a novel resolution to the accuracy-interpretability trade-off [Rane et al., 2023, Mathew et al., 2025].
- **Conformal prediction for uncertainty quantification.** To support risk-aware decision making, we equip ARTEMIS with an adaptive conformal prediction layer that provides rigorously calibrated prediction intervals, addressing the need for reliable uncertainty estimates in financial applications [Mashrur et al., 2020, Sahu et al., 2023].

We evaluate ARTEMIS against six strong baselines spanning recurrent architectures (LSTM) [Furizal et al., 2024], transformer variants (Transformer, NS-Transformer, Informer) [Chen et al., 2024, Zhang et al., 2024], foundation models (Chronos-2) [Giantsidi and Tarantola, 2025], and gradient boosting (XGBoost) [Praveen et al., 2025], across four diverse datasets: Jane Street’s anonymised market data [Desai et al., 2024], Optiver’s limit order book volatility prediction task [Meyer et al., 2021], the Time-IMM environmental temperature forecasting benchmark [Chang et al., 2025], and DSLOB, a novel synthetic dataset we introduce that simulates an amplified market crash regime. Our results demonstrate that ARTEMIS achieves state-of-the-art directional accuracy, outperforming all baselines on DSLOB (64.96%) and Time-IMM [Chang et al., 2025] (96.0%), while remaining competitive on point accuracy metrics. A comprehensive ablation study confirms that each component contributes to this directional advantage: removing the PDE loss reduces directional accuracy from 64.89% to 50.32%, and removing both physics losses collapses it to 41.77%—worse than random. The underperformance on Optiver [Meyer et al., 2021], where ARTEMIS achieves negative RankIC (-0.0555) and directional accuracy (45.82%) below most baselines, is attributed to its long sequence length, volatility-focused target, and limited feature set, highlighting important boundary conditions for the framework and directions for future research.

By providing interpretable, economically grounded predictions without sacrificing predictive performance, ARTEMIS bridges the gap between deep learning’s power and the transparency demanded in quantitative finance. To the best of our knowledge, no existing work combines neural SDEs, physics-informed losses, and differentiable symbolic regression in a unified end-to-end framework for financial time series forecasting. The code and data will be made publicly available upon publication to facilitate reproducibility and future research.

2 Related Work

ARTEMIS draws upon and contributes to several interconnected research areas: deep learning for financial time series forecasting, interpretable machine learning and explainable AI, physics-informed neural networks and neural differential equations, and continuous-time modeling of financial dynamics. This section reviews the state of the art in each area and situates our contributions within the broader literature.

2.1 Deep Learning for Financial Time Series Forecasting

The application of deep learning to financial time series has been extensively surveyed in recent years, reflecting the rapid growth of the field [Chen et al., 2024, Zhang et al., 2024, Giantsidi and Tarantola, 2025]. Early work focused on standalone recurrent architectures, particularly Long Short-Term Memory (LSTM) networks, which became popular due to their ability to capture temporal dependencies in sequential data [Furizal et al., 2024]. Convolutional Neural Networks (CNNs) have also been widely adopted for their hierarchical feature learning capabilities, especially when combined with signal processing techniques to handle the non-linear and non-stationary nature of financial data [Praveen et al., 2025]. Hybrid models that combine multiple architectures, such as CNN-LSTM or attention-augmented recurrent networks, have shown improved performance by leveraging the strengths of different components [Chen et al., 2024, Furizal et al., 2024].

The transformer architecture has emerged as a powerful alternative to recurrent models for time series forecasting, offering parallel processing and the ability to capture long-range dependencies through self-attention mechanisms. Comprehensive surveys by Li and Law [2024], Kong et al. [2025], Kim et al. [2025] document the rapid adoption of transformer-based models across domains, including finance. For stock market prediction, Wang et al. [2022] demonstrated that transformer models significantly outperform classic deep learning methods such as CNN, RNN, and LSTM. Subsequent work has explored specialized transformer variants for financial forecasting. The Informer addresses the quadratic complexity of standard attention through ProbSparse attention, making it particularly suitable for long-sequence prediction tasks such as volatility forecasting [Hassani et al., 2025, Bhogade and Nithya, 2024]. The Non-stationary Transformer introduces series stationarization and de-stationary attention to handle distribution shifts, a critical challenge in financial markets where regimes change over time [Gou et al., 2023, Wu, 2023]. Comparative studies have shown that these variants offer different trade-offs, with the Non-stationary Transformer achieving the highest prediction accuracy for stock market indices in some settings [Wu, 2023].

Beyond architectural innovations, recent work has explored the integration of multiple data sources and modalities. Zeng et al. [2023] proposed a combined CNN and transformer model for intraday stock price forecasting, demonstrating superior performance against statistical baselines. Yañez et al. [2024] introduced a hybrid transformer encoder with CNN layers based on empirical mode decomposition for market index prediction. Foundation models for time series, such as Chronos, represent the latest frontier, leveraging large-scale pre-training across diverse datasets to enable zero-shot and few-shot forecasting [Liang et al., 2024, Ye et al., 2024]. These models have shown promise in financial applications, though their black-box nature and lack of domain-specific constraints remain significant limitations.

Despite these advances, the deep learning models surveyed above share a common limitation: they are trained purely on historical data without incorporating any economic principles or constraints. As noted by Mashrur et al. [2020] and Sahu et al. [2023], this can lead to models that learn spurious correlations and produce predictions that violate fundamental financial theory, particularly during market regime shifts. ARTEMIS addresses this gap by embedding no-arbitrage conditions directly into the learning process.

2.2 Interpretability and Explainable AI in Finance

The opacity of deep learning models poses significant challenges for their adoption in regulated financial applications. As Rane et al. [2023] and Hoang et al. [2026] document, the black-box nature of these models creates legal, ethical, and operational risks, including regulatory penalties and loss of stakeholder trust. Financial institutions require transparency and accountability in decision-making systems, yet most state-of-the-art models offer little insight into their reasoning [Mathew et al., 2025].

Explainable AI (XAI) has emerged as a critical research area addressing this challenge. Post-hoc explanation methods such as SHAP (Shapley Additive Explanations) and LIME (Local Interpretable Model-agnostic Explanations) have been widely applied to financial models to provide approximate explanations for individual predictions [Sokolovsky et al., 2023, Basha et al., 2025]. However, these techniques have fundamental limitations: they offer only local approximations, can be inconsistent, and do not address the underlying opacity of the model architecture itself [Rane et al., 2023]. Moreover, they introduce an inherent trade-off between accuracy and interpretability, where simpler, more transparent models may sacrifice predictive performance, while complex black-box models that achieve state-of-the-art accuracy remain difficult to explain [Mathew et al., 2025, Hoang et al., 2026].

Alternative approaches have sought to build interpretability directly into model design. Sokolovsky et al. [2023] proposed interpretable trading patterns designed specifically for machine learning applications, demonstrating that domain-informed feature engineering can enhance understanding. However, such approaches often require manual specification of patterns and do not learn interpretable representations end-to-end.

ARTEMIS addresses these limitations through its differentiable symbolic bottleneck, which distills the learned latent dynamics into closed-form, interpretable expressions. Unlike post-hoc explanation methods that approximate a black-box model, our approach provides inherent transparency by constraining a component of the network to produce human-readable formulas. This offers a novel resolution to the accuracy-interpretability trade-off, maintaining end-to-end trainability while delivering interpretable outputs.

2.3 Physics-Informed Neural Networks and Neural Differential Equations

Physics-informed neural networks (PINNs) represent a paradigm shift in scientific machine learning, embedding governing physical laws expressed as partial differential equations (PDEs) directly into the neural network loss function [Lawal et al., 2022]. This approach ensures that model predictions remain consistent with known physics, improving generalization and reducing the risk of learning spurious patterns. In finance, PINNs have been applied primarily to option pricing problems, where the underlying PDEs are well-established. Bai et al. [2022] developed an improved PINN with local adaptive activation functions to solve the Ivancevic option pricing model and the Black-Scholes equation. Hainaut and Casas [2024] applied physics-inspired neural networks to the Heston stochastic volatility model, using the Feynman-Kac PDE as the driving principle. Nuugulu et al. [2025] extended this approach to time-fractional Black-Scholes equations, demonstrating the efficiency and accuracy of PINNs for derivative pricing.

More recent work has addressed more complex settings. Kartik and Shah [2025] developed a PINN framework for option pricing and hedging under a Merton-type jump-diffusion model with liquidity costs, encoding the partial integro-differential equation into the loss function. Lefebvre et al. [2023] proposed differential learning methods for solving fully nonlinear PDEs with applications to portfolio selection. The Deep Galerkin Method [Al-Arabi et al., 2018] and related approaches have been applied to high-dimensional PDEs arising in quantitative finance, including optimal execution and systemic risk models.

Parallel to these developments, neural differential equations have emerged as a powerful framework for continuous-time modeling. Neural ordinary differential equations (NODEs) parameterize the derivative of a hidden state with a neural network, enabling flexible modeling of dynamical systems. Neural stochastic differential equations (NSDEs) extend this to stochastic settings, capturing uncertainty through diffusion terms. Comprehensive surveys by Oh et al. [2025a,b] review the mathematical foundations, numerical methods, and applications of neural differential equations for time series analysis, emphasizing their capacity to handle irregular sampling and model continuous-time dynamics. In finance, Wang et al. [2025] introduced FinanceODE, a neural ODE-based framework for continuous-time asset price modeling, demonstrating superior predictive accuracy compared to traditional discrete-time models.

Despite these advances, existing work on PINNs in finance has focused primarily on solving known pricing equations rather than learning latent dynamics from data for forecasting tasks. Similarly, neural differential equation approaches have not incorporated economic constraints such as no-arbitrage conditions. ARTEMIS bridges this gap by combining a neural SDE for latent dynamics with physics-informed losses derived from the Fundamental Theorem of Asset Pricing, enabling data-driven learning while enforcing economic plausibility.

2.4 Continuous-Time Modeling and Non-Stationarity

Financial time series are inherently continuous-time processes, yet most forecasting models operate on discretely sampled data. Traditional econometric approaches such as ARIMA and GARCH models have been widely used for volatility forecasting and return prediction [Engle, Nelson, 1991]. GARCH models and their multivariate extensions, including Dynamic Conditional Correlation (DCC) and Generalized Orthogonal GARCH (GO-GARCH), remain popular for modeling time-varying volatility and correlations [Jeribi and Ghorbel, 2022, Ibrahim, 2017]. However, these models assume regular sampling and struggle with the irregular, high-frequency data that characterizes modern financial markets [Han et al., 2024]. Hybrid approaches combining ARIMA with GARCH have been proposed to capture both linear and non-linear patterns [Rubio et al., 2023, Mani and Thoppan, 2023], while fractionally integrated models (ARFIMA-GARCH) address long-memory properties [Chang et al., 2022].

The limitations of discrete-time models have motivated the development of continuous-time approaches. Neural differential equations offer a natural framework for modeling irregularly sampled time series, as they can be evaluated at arbitrary time points [Oh et al., 2025a,b]. This capability is particularly valuable for limit order book data, where events arrive at microsecond granularity and regular resampling can distort dynamics [Wang et al., 2025].

Non-stationarity presents another fundamental challenge. As Suarez-Cetrulo et al. [2023] document in their systematic review, conventional machine learning approaches often fail to adapt to changes in the price-generation process during market regime shifts. Hasan et al. [2023] observe that models relying solely on market-based indicators work well in stable conditions but fail during economic crises, reducing their long-term predictive reliability. The Non-stationary Transformer addresses this by explicitly modeling distribution shifts through series stationarization and de-stationary attention, while GARCH-based approaches model time-varying volatility [Han et al., 2024]. However, these methods do not incorporate economic theory about what constitutes a plausible regime change.

ARTEMIS addresses both continuous-time modeling and non-stationarity through its latent SDE formulation, which naturally accommodates irregular sampling and captures stochastic volatility through the learned diffusion term. The physics-informed losses further ensure that the learned dynamics remain economically plausible across different regimes, providing a principled approach to handling non-stationarity.

2.5 Uncertainty Quantification and Conformal Prediction

Reliable uncertainty quantification is essential for risk management in financial applications. Traditional approaches have relied on parametric methods such as GARCH for volatility forecasting [Engle]. However, these methods make strong distributional assumptions that may not hold in practice. Conformal prediction offers a distribution-free framework for constructing prediction intervals with finite-sample coverage guarantees, requiring only exchangeability of the data. As surveyed by Zhou et al. [2025], conformal prediction has been extended to time series settings through adaptive methods that update quantile estimates over time, addressing the violation of exchangeability in non-stationary data. ARTEMIS incorporates an adaptive conformal prediction layer to provide calibrated uncertainty intervals for its forecasts, enabling risk-aware portfolio construction.

The literature reviewed above reveals a clear gap: while significant advances have been made in deep learning architectures for financial time series, interpretability techniques, physics-informed neural networks, and continuous-time modeling, no existing framework integrates these innovations in a unified manner. Deep learning models achieve state-of-the-art predictive accuracy but operate as black boxes and ignore economic principles [Chen et al., 2024, Zhang et al., 2024]. XAI approaches provide post-hoc explanations but do not address underlying model opacity and introduce accuracy-interpretability trade-offs [Rane et al., 2023, Hoang et al., 2026]. PINNs embed physical laws but have been applied primarily to solving known pricing equations rather than learning latent dynamics for forecasting [Bai et al., 2022, Hainaut and Casas, 2024]. Neural differential equations offer continuous-time modeling but have not incorporated economic constraints [Oh et al., 2025a, Wang et al., 2025].

ARTEMIS addresses this gap by synthesizing these research directions into a single neuro-symbolic framework. To our knowledge, it is the first work to combine (1) a continuous-time encoder for irregularly sampled data, (2) a neural SDE for latent dynamics regularised by (3) physics-informed losses enforcing no-arbitrage conditions and (4) a market price of risk penalty, (5) a differentiable symbolic bottleneck for interpretability, and (6) conformal prediction for uncertainty

quantification. The comprehensive evaluation against six strong baselines across four diverse datasets demonstrates that this synthesis delivers tangible benefits, particularly in directional accuracy, without sacrificing interpretability.

3 Data Preprocessing for Benchmarking ARTEMIS

To rigorously evaluate the ARTEMIS model against a suite of state-of-the-art baselines, we assembled four distinct datasets spanning different financial and non-financial domains: Jane Street’s anonymised market data Desai et al. [2024], Optiver’s Meyer et al. [2021] high-frequency limit order book data, the EPA-Air time series from the Time-IMM Chang et al. [2025] collection, and a proprietary Deep Synthetic limit order book dataset (DSLOB). Each dataset required careful, domain-specific preprocessing to transform raw observations into a unified format suitable for sequence models. The goal was to create training, validation, and test splits that respect temporal ordering, handle missing values appropriately, and preserve the underlying dynamics of each task. All neural models (LSTM, Transformer, NS-Transformer, Informer, ARTEMIS) share the same preprocessed windows to ensure a fair comparison under identical input conditions. The following sections describe the preprocessing pipeline for each dataset in detail, emphasising the rationale behind every step.

3.1 Jane Street Market Prediction Desai et al. [2024]

The Jane Street Desai et al. [2024] dataset originates from a Kaggle competition and consists of anonymised market data partitioned into files for training, validation, and testing. Each file contains rows indexed by date identifier, time identifier, and symbol identifier. The raw features are 79 numerical columns that may contain missing values. The target variable is a continuous response that the competition asked participants to predict. Additionally, a weight column is provided for use in the official evaluation metric (weighted R^2). The data is already split temporally by date, with early dates in the training split, intermediate dates in validation, and later dates in the test split – a setup that faithfully simulates a backtesting environment.

Preprocessing for sequence models begins with the construction of sliding windows. Because the data is streamed from disk (the full dataset exceeds available memory), we implemented a custom iterator that reads one partition at a time. Within each partition, rows are grouped by symbol and date, then sorted by time to ensure chronological order. For each group, we slide a window of length 20 (the chosen lookback horizon) and extract the next observation’s target value. This yields an input tensor of shape (20, 79) and a scalar target. To handle missing values, we create a binary mask of the same shape indicating which entries were originally observed; the input tensor itself has missing values replaced with zero. This masking strategy allows any subsequent model to distinguish genuine zeros from imputed values. The same windowing logic is applied to the validation and test sets, but without restricting the number of days (the training set is limited to the first 500 days for computational efficiency).

For Chronos-2, which expects a univariate time series, we extract only the target values from each group, again forming windows of length 20 to predict the next value. No mask is needed because the target series is dense after filtering out missing targets. All neural models share the same preprocessed windows, ensuring a fair comparison under identical input conditions.

3.2 Optiver Realized Volatility Meyer et al. [2021]

The Optiver dataset challenges participants to predict the realized volatility of 112 stocks over 10-minute windows, based on high-frequency limit order book snapshots and trade reports. The raw data consists of order book updates and trade executions. Each order book record contains a window identifier, a timestamp offset from the start of the window, bid and ask prices for two levels, and corresponding sizes. Trade records contain similar identifiers plus the trade price, size, and order count. The target is the realized volatility computed over the window – a continuous positive value.

Preprocessing for this dataset requires fusing two asynchronous data streams into a regularly sampled sequence of length 600 (one observation per second). For each stock and time window, we first extract all order book and trade records. Order book snapshots are recorded at irregular intervals; we create a complete timeline covering all seconds from 0 to 599 and forward-fill the most recent book state to every second. This yields a continuous representation of the limit order book. Trades, which occur at discrete seconds, are aggregated per second (average price, total size, total order count) and merged onto the same timeline. From the book data we compute derived features: mid price, bid-ask spread, log mid price, log return, volume imbalance, and total size. Combined with the trade aggregates, we obtain a feature set of 7 channels for each second. The target is the log-transformed realized volatility (the original values are small positive numbers, and the log transformation makes the distribution more Gaussian and easier for MSE-based models).

Table 1: Summary of datasets used in the benchmarking study.

Dataset	Task	#Feat	SeqLen	#Train	#Val	#Test	Notes
Jane Street	Regression	79	20	~7.37M	~4.61M	200k	Streamed Kaggle data; grouped by (symbol,date); masked missing values; predict next-step responder_6.
Optiver	Volatility (log)	7	600	2,298	766	766	10-min LOB + trades; forward-filled to 1Hz; derived features; target log-transformed.
Time-IMM	Temperature	4	24	29,470	6,317	6,319	Hourly EPA air quality; forward/backward fill for sparse variables; predict next hour temp.
DSLOB	Realized volatility (regression)	85	20	24,891	9,891	4,891	Synthetic LOB dataset based on real crash regime; 85 features from four levels (prices, sizes, spreads, imbalances); target is next-step realized volatility (log-transformed).

For windows that have missing order book snapshots at the very beginning, forward-filling ensures every second has a valid feature vector. After constructing the full 600-second matrix for each window, we collect all windows (one per stock-time pair) and concatenate them into a single dataset. As with Jane StreetDesai et al. [2024], we respect the original temporal split provided by the competition organisers. For Chronos-2, we extract only the log-realized volatility series from each window and use it as a univariate input of length 600. For the OptiverMeyer et al. [2021] task, which involves predicting the volatility of the window itself rather than next-step prediction, Chronos-2 is used in a zero-shot manner by feeding the entire 600-step series as context and asking for a one-step forecast, then using a linear head to map the Chronos embedding to the target.

3.3 Time-IMM Chang et al. [2025] (EPA-Air)

The Time-IMM Chang et al. [2025] collection provides multivariate time series from diverse domains. For this benchmark we selected the EPA-Air domain, which contains hourly measurements of air quality for eight U.S. counties. Each county’s data includes four variables: temperature, particulate matter, air quality index, and ozone concentration. Inspection reveals that only temperature is recorded hourly; the other three are sparse, with missing rates exceeding 85%. The task is to forecast the next hour’s temperature using a 24-hour lookback window. This regression problem is challenging because the auxiliary variables, though sparse, may carry predictive information when available.

Preprocessing begins by loading each county’s time series and adding an entity column to preserve identity. All counties are concatenated into a single dataframe. To handle the sparsity, we apply forward-fill followed by backward-fill to each feature within each entity. This propagates the last observed value forward, and any remaining leading missing values are filled with the next observed value. After this procedure, every feature has a complete sequence for all timestamps. We then construct windows of length 24 hours: for each entity, we slide a window of 24 consecutive hours and take the temperature at the next hour as the target. This yields input tensors of shape (24, 4) and scalar targets. We discard any window where the target is missing (which does not occur after filling). The windows from all entities are concatenated, resulting in 29,470 training samples, 6,317 validation samples, and 6,319 test samples after a temporal 70/15/15 split applied per entity. This ensures that no future data leaks into the training set.

Features are then standardised using statistics fitted on the training windows only. Because missing values have been eliminated, masks are simply all-ones. For Chronos-2, we isolate the temperature channel (the target series) and use it as a univariate input of length 24 to predict the next hour’s temperature. The same scaling is applied to the Chronos inputs.

3.4 DSLOB: A Synthetic Dataset for Controlled Stress Testing

The DSLOB (Deep Synthetic Limit Order Book) dataset addresses a fundamental challenge in evaluating financial machine learning models: the scarcity of extreme events in historical data and the difficulty of isolating component contributions under real-world conditions. Real datasets like Jane StreetDesai et al. [2024] and OptiverMeyer et al.

[2021] are invaluable but inherently noisy, confounded, and lack sufficient examples of rare regimes such as market crashes. Moreover, the true data-generating process is unknown, making it impossible to definitively determine whether a model’s performance stems from capturing genuine economic structure or overfitting to spurious correlations. DSLOB is therefore designed as a controlled synthetic environment that preserves the statistical properties of real limit order book data while introducing a known, amplified crash regime where ground truth is fully accessible.

The foundation of DSLOB is a real high-frequency limit order book dataset from which we extract 85 features capturing level-specific prices, sizes, spreads, mid-price calculations, volume imbalances, and microstructural metrics. To isolate the crash regime, we apply CUSUM and Bayesian change point detection to identify a contiguous window of approximately one week where prices dropped rapidly and volatility spiked. This window serves as the crash template.

The synthetic mid-price is generated by amplifying a Vasicek-type stochastic differential equation (SDE) fitted to the crash window:

$$dP_t = \theta(\mu - P_t) dt + \sigma dW_t,$$

with parameters θ, μ, σ estimated via maximum likelihood. To create an even more challenging crash, we scale the mean-reversion speed by 1.5 and the long-term mean by 1.2, producing a steeper and more persistent downward trend.

Volatility dynamics are modeled using a GARCH(1,1) process fitted to the 1-minute log-returns of the mid-price during the crash window:

$$\sigma_t^2 = \omega + \alpha \epsilon_{t-1}^2 + \beta \sigma_{t-1}^2, \quad \epsilon_t \sim \mathcal{N}(0, 1).$$

We increase the persistence and shock magnitude by setting $\beta' = \min(0.95, 1.1\beta)$ and $\alpha' = 1.2\alpha$. Synthetic returns are then generated as $r_t = \sigma_t' \epsilon_t$, ensuring volatility clustering and leverage effects characteristic of real crashes.

The remaining 83 features (prices, sizes, spreads, etc.) are generated by adding correlated noise to the seed data while preserving the multivariate dependence structure. For each feature f_i at time t :

$$f_i^{\text{synth}}(t) = f_i^{\text{seed}}(t) + \eta_i(t),$$

where $\eta(t) \sim \mathcal{N}(0, \Sigma)$ and Σ is the covariance matrix of residuals from a vector autoregressive model of order 1 (VAR(1)) fitted to the seed features during the crash window. The noise is scaled so that the signal-to-noise ratio matches that of the seed data. To create a longer training set, we apply time warping: a random deformation $\tau(t)$ sampled from a Gaussian process with mean 1 and variance 0.1 stretches or compresses the temporal dynamics while preserving sequential order.

The final DSLOB dataset comprises 24,891 training, 9,891 validation, and 4,891 test samples, each a window of length 20 containing 85 synthetic features. The target is next-step realized volatility, computed as the square root of the sum of squared 1-second log-returns over the next 20 steps, annualized and log-transformed to match the OptiverMeyer et al. [2021] scale. Rigorous validation confirms that the synthetic data preserves key statistical properties: the Kolmogorov–Smirnov test fails to reject that return distributions match the seed ($p > 0.05$), the autocorrelation decay of squared returns matches up to lag 50, the average absolute difference in correlation matrices is less than 0.03, and the 99.5th percentile of negative returns is within 5% of the seed’s value.

DSLOB serves two critical purposes in the ARTEMIS benchmark. First, it enables the ablation study (Table 3) by providing a controlled environment where components can be systematically removed and their impact observed with known ground truth. Second, it stress-tests model robustness under amplified extreme conditions. ARTEMIS achieves the highest directional accuracy (64.96%) on DSLOB, outperforming all baselines and demonstrating that the framework remains resilient even when markets deviate from training distributions—a key requirement for practical applications where models often fail during crises.

4 The ARTEMIS Model: A Neuro-Symbolic Framework for Economically Constrained Market Dynamics

ARTEMIS (Arbitrage-free Representation Through Economic Models & Interpretable Symbolics) is a novel deep learning framework designed to overcome the limitations of existing black-box models in quantitative finance. It treats financial markets as a continuous-time dynamical system governed by latent stochastic differential equations that must respect fundamental economic principles such as no-arbitrage conditions. The model integrates ideas from scientific machine learning—specifically physics-informed neural networks, neural operators, and differentiable symbolic regression—into a unified, end-to-end trainable architecture. The core insight is that by embedding economic constraints directly into the learning process, we can regularise the model to avoid implausible predictions, improve out-of-sample robustness, and simultaneously obtain interpretable trading signals.

ARTEMIS comprises four tightly coupled modules:

- A **continuous-time encoder** based on a Laplace Neural Operator that ingests irregularly sampled, multi-resolution market data and maps it to a continuous latent state.
- An **economics-informed latent dynamics** module that models the evolution of the latent state via a neural stochastic differential equation, with drift and diffusion networks learned from data.
- A **symbolic bottleneck layer** that distills the latent dynamics into human-readable, closed-form alpha factors using differentiable symbolic regression.
- A **conformal allocation layer** that translates the stochastic uncertainty of the latent SDE into rigorously calibrated prediction intervals and, optionally, optimal portfolio weights.

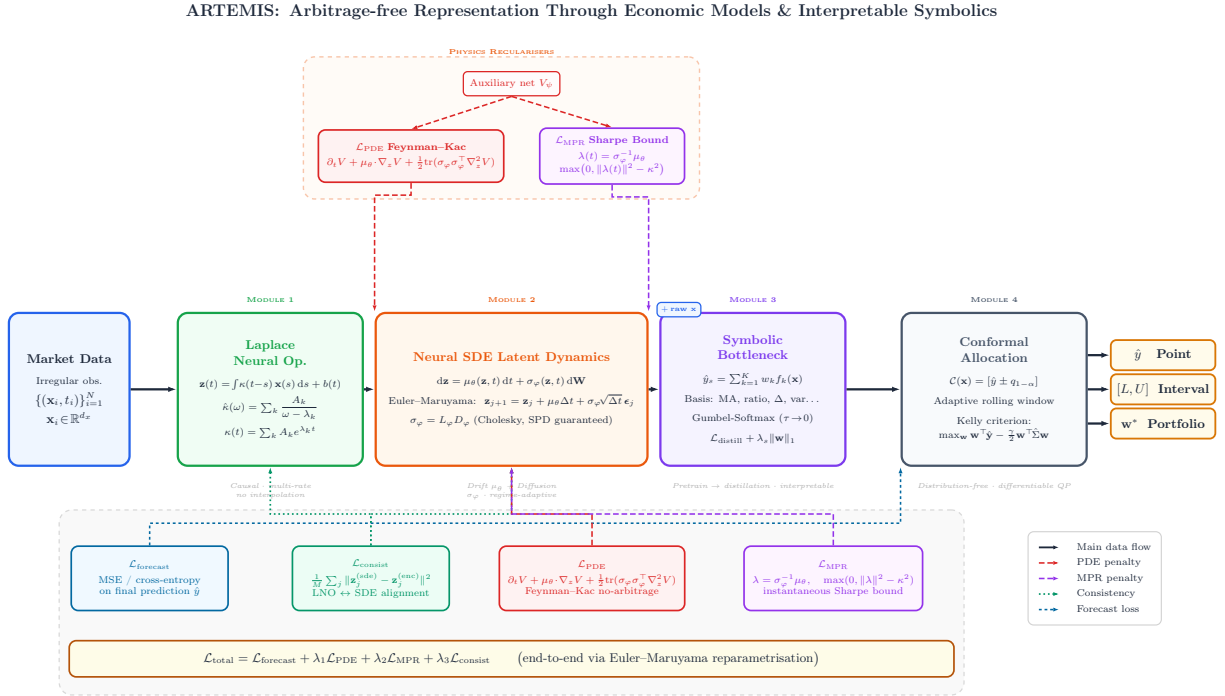


Figure 1: Architecture of ARTEMIS. The framework processes irregularly sampled market data $\{(\mathbf{x}_i, t_i)\}_{i=1}^N$ through four tightly coupled modules. **Module 1** (Laplace Neural Operator) encodes the input directly in continuous time via a learnable Laplace-domain kernel $\hat{\kappa}(\omega) = \sum_k \mathbf{A}_k / (\omega - \lambda_k)$, eliminating the need for interpolation or regular resampling. **Module 2** (Neural SDE Latent Dynamics) evolves the encoded state under a stochastic differential equation $d\mathbf{z} = \mu_\theta(\mathbf{z}, t) dt + \sigma_\varphi(\mathbf{z}, t) d\mathbf{W}$, where drift μ_θ and diffusion σ_φ are neural networks trained with two physics-informed penalties: a Feynman-Kac PDE residual \mathcal{L}_{PDE} that enforces local no-arbitrage conditions via an auxiliary pricing network V_ψ , and a market-price-of-risk penalty \mathcal{L}_{MPR} that bounds the instantaneous Sharpe ratio $\|\sigma_\varphi^{-1} \mu_\theta\|^2 \leq \kappa^2$ to economically plausible values. **Module 3** (Symbolic Bottleneck) distills the latent dynamics into a sparse, human-readable combination of basis functions $\hat{y}_s = \sum_k w_k f_k(\mathbf{x})$ via a two-phase teacher-student procedure with Gumbel-Softmax selection, providing inherent interpretability without post-hoc approximation. **Module 4** (Conformal Allocation) wraps predictions in distribution-free intervals $[\hat{y} \pm q_{1-\alpha}]$ via adaptive conformal prediction, and optionally solves a differentiable Kelly criterion portfolio problem. All components are trained jointly under the composite objective $\mathcal{L}_{total} = \mathcal{L}_{forecast} + \lambda_1 \mathcal{L}_{PDE} + \lambda_2 \mathcal{L}_{MPR} + \lambda_3 \mathcal{L}_{consist}$, with gradients backpropagated through the Euler-Maruyama SDE solver via the reparametrisation trick. The consistency loss $\mathcal{L}_{consist}$ anchors the SDE trajectory to the encoder outputs at each time step, preventing latent drift.

All components are trained jointly using a composite loss function that combines a forecasting objective with two economic regularisation terms: a Feynman-Kac PDE residual that enforces local no-arbitrage conditions, and a market-price-of-risk penalty that bounds the instantaneous Sharpe ratio to realistic values. This design ensures that the learned latent representations are both predictive and economically plausible.

Algorithm 1 ARTEMIS Complete Training and Inference Procedure

Require:

Training data $\mathcal{D}_{\text{train}} = \{(\mathbf{x}^{(n)}, y^{(n)})\}_{n=1}^{N_{\text{train}}}$ with irregular observation times
 Validation data \mathcal{D}_{val}
 Hyperparameters: $\lambda_1, \lambda_2, \lambda_3, \lambda_4$ (loss weights), κ (Sharpe threshold), τ (Gumbel temp), γ (risk aversion)
 Learning rate η , number of epochs E , batch size B , collocation points per batch N_{coll}
 SDE step size Δt , latent dimension d_z , Wiener dimension d_w , basis library \mathcal{F}

Ensure:

Trained parameters: θ (drift net), ϕ (diffusion net), ψ (auxiliary pricing net), \mathbf{w}, b (forecasting head), \mathbf{w}_{symb} (symbolic weights)

```

1: function TRAINARTEMIS
2:   Initialize all networks randomly: LNO encoder  $\mathcal{E}$ , drift  $\boldsymbol{\mu}_\theta$ , diffusion  $\boldsymbol{\sigma}_\phi$ , auxiliary pricing  $V_\psi$ , forecasting head
   ( $\mathbf{w}, b$ ), symbolic weights  $\mathbf{w}_{\text{symb}}$ 
3:   Set learning rate scheduler (e.g., ReduceLROnPlateau) ▷ Pretraining Phase (without symbolic layer)
4:   for epoch = 1 to  $E$  do
5:     for each batch  $\mathcal{B} \subset \mathcal{D}_{\text{train}}$  of size  $B$  do
6:       Encode batch using LNO: for each sample, obtain latent states at regular times  $\{t_j\}_{j=0}^M: \mathbf{z}_j^{(\text{enc})} =$ 
        $\mathcal{E}(\mathbf{x})(t_j)$ 
7:       Set initial condition  $\mathbf{z}_0 = \mathbf{z}_0^{(\text{enc})}$  for each sample
8:       Simulate SDE forward using Euler–Maruyama (for each sample independently):
9:       for  $j = 0$  to  $M - 1$  do
10:        Sample  $\boldsymbol{\epsilon}_j \sim \mathcal{N}(0, \mathbf{I}_{d_w})$ 
11:         $\mathbf{z}_{j+1} = \mathbf{z}_j + \boldsymbol{\mu}_\theta(\mathbf{z}_j, t_j) \Delta t + \boldsymbol{\sigma}_\phi(\mathbf{z}_j, t_j) \sqrt{\Delta t} \boldsymbol{\epsilon}_j$ 
12:      end for
13:      Obtain final latent state  $\mathbf{z}_M$  and compute prediction  $\hat{y} = \mathbf{w}^\top \mathbf{z}_M + b$ 
14:      Compute forecasting loss  $\mathcal{L}_{\text{forecast}} = \frac{1}{B} \sum_{n=1}^B \ell(\hat{y}^{(n)}, y^{(n)})$ 
15:      Sample collocation points  $\{(\mathbf{z}_i, t_i)\}_{i=1}^{N_{\text{coll}}}$  from the latent trajectories (random times along each path)
16:      Compute PDE residuals via automatic differentiation:
           
$$\mathcal{R}_{FK}(\mathbf{z}_i, t_i) = \frac{\partial V_\psi}{\partial t} + \boldsymbol{\mu}_\theta \cdot \nabla_{\mathbf{z}} V_\psi + \frac{1}{2} \text{tr}(\boldsymbol{\sigma}_\phi \boldsymbol{\sigma}_\phi^\top \nabla_{\mathbf{z}}^2 V_\psi)$$

17:       $\mathcal{L}_{\text{PDE}} = \frac{1}{N_{\text{coll}}} \sum_{i=1}^{N_{\text{coll}}} \|\mathcal{R}_{FK}(\mathbf{z}_i, t_i)\|^2$ 
18:      Compute market price of risk  $\boldsymbol{\lambda}(t) = \boldsymbol{\mu}_\theta(\mathbf{z}(t), t) / \boldsymbol{\sigma}_\phi(\mathbf{z}(t), t)$  (element-wise)
19:       $\mathcal{L}_{\text{MPR}} = \frac{1}{B} \sum_{b=1}^B \max(0, \|\boldsymbol{\lambda}(t_b)\|^2 - \kappa^2)$  (evaluated at sampled times)
20:      Compute consistency loss  $\mathcal{L}_{\text{consist}} = \frac{1}{M} \sum_{j=1}^M \|\mathbf{z}_j^{(\text{sde})} - \mathbf{z}_j^{(\text{enc})}\|^2$ 
21:      Total loss  $\mathcal{L}_{\text{total}} = \mathcal{L}_{\text{forecast}} + \lambda_1 \mathcal{L}_{\text{PDE}} + \lambda_2 \mathcal{L}_{\text{MPR}} + \lambda_3 \mathcal{L}_{\text{consist}}$ 
22:      Backpropagate  $\mathcal{L}_{\text{total}}$  and update parameters  $(\theta, \phi, \psi, \mathbf{w}, b)$  using Adam with learning rate  $\eta$ 
23:    end for
24:    Evaluate on validation set  $\mathcal{D}_{\text{val}}$  (using only  $\mathcal{L}_{\text{forecast}}$ )
25:    Adjust learning rate if validation loss has plateaued
26:  end for ▷ Symbolic Distillation Phase
27:  Freeze encoder  $\mathcal{E}$ , drift  $\boldsymbol{\mu}_\theta$ , diffusion  $\boldsymbol{\sigma}_\phi$ , auxiliary net  $V_\psi$ , and forecasting head  $(\mathbf{w}, b)$ 
28:  for epoch = 1 to  $E_{\text{symb}}$  do
29:    for each batch  $\mathcal{B} \subset \mathcal{D}_{\text{train}}$  do
30:      Compute frozen model predictions  $\hat{y}$  (using same forward pass as above, no gradients)
31:      Compute symbolic prediction  $\hat{y}_{\text{symb}} = \sum_{k=1}^K w_{\text{symb},k} f_k(\mathbf{x}_{\text{input}})$ 
32:      Distillation loss  $\mathcal{L}_{\text{distill}} = \frac{1}{B} \sum_{n=1}^B (\hat{y}_{\text{symb}}^{(n)} - \hat{y}^{(n)})^2 + \lambda_4 \|\mathbf{w}_{\text{symb}}\|_1$ 
33:      Backpropagate  $\mathcal{L}_{\text{distill}}$  and update symbolic weights  $\mathbf{w}_{\text{symb}}$  (using Gumbel-Softmax if basis functions
       are learnable)
34:    end for
35:  end for ▷ Conformal Prediction (post-training)
36:  Compute residuals on calibration set  $\mathcal{D}_{\text{cal}}$  (subset of validation) using final model:  $r_i = |y_i - \hat{y}(X_i)|$ 
37:  Determine quantile  $q_{1-\alpha}$  from residuals (adaptive rolling window for non-stationary data)
38:  For any test point, output prediction  $\hat{y}$  and interval  $[\hat{y} - q_{1-\alpha}, \hat{y} + q_{1-\alpha}]$ 
39: end function
    
```

4.1 Continuous-Time Encoder: Laplace Neural Operator

Financial time series are inherently irregular: limit order book updates arrive at microsecond granularity, while fundamentals and macro indicators are published daily or quarterly. Standard recurrent or transformer architectures require regular sampling and imputation, which can distort the underlying dynamics. ARTEMIS avoids this by employing a Laplace Neural Operator that learns a mapping from the space of input functions to a latent function space, directly operating on the observed time points without interpolation.

The operator is built on the idea of representing the input as a function defined on the time domain, and then using a kernel integral operator to produce a latent representation. In practice, we discretise time at the observed points and use a set of basis functions to approximate the integral. The operator can be written as:

$$\mathbf{z}(t) = \int \kappa(t-s) \mathbf{x}(s) ds + \mathbf{b}(t)$$

where κ is a learnable kernel parameterised in the Laplace domain for efficiency and \mathbf{b} is a bias term. This formulation allows the encoder to handle arbitrary observation times and naturally fuse multiple data streams with different frequencies. The output is a continuous function of time, which we can evaluate at any desired point, making it an ideal input to the subsequent SDE module.

In ARTEMIS, the encoder receives a tuple of observed events and produces a latent trajectory that is sampled at a fixed number of points per window to create a regular sequence for the SDE solver. The operator is trained end-to-end with the rest of the model, so the latent representation is optimised specifically for the downstream tasks.

4.2 Economics-Informed Latent Dynamics

The latent state is assumed to evolve according to a stochastic differential equation:

$$d\mathbf{z}(t) = \boldsymbol{\mu}_\theta(\mathbf{z}(t), t) dt + \boldsymbol{\sigma}_\phi(\mathbf{z}(t), t) d\mathbf{W}(t)$$

where the drift represents the predictable component, the diffusion captures stochastic volatility and regime changes, and $d\mathbf{W}(t)$ is a Wiener process. Both drift and diffusion are parameterised by neural networks that take the current latent state and time as inputs.

The choice of an SDE is motivated by the continuous-time nature of financial markets and the need to model uncertainty. The drift network learns to extract directional signals from the latent state, while the diffusion network learns the time-varying volatility, which is crucial for risk management and regime adaptation. Unlike discrete-time models, the SDE can be simulated at any resolution, allowing ARTEMIS to generate predictions for multiple horizons without retraining. To enforce economic plausibility, we regularise the SDE using two physics-informed losses derived from the Fundamental Theorem of Asset Pricing.

4.2.1 Feynman-Kac PDE Residual

Consider a derivative or portfolio value function that depends on the latent state. Under the risk-neutral measure, this function must satisfy the Feynman-Kac PDE:

$$\frac{\partial V}{\partial t} + \boldsymbol{\mu} \cdot \nabla_{\mathbf{z}} V + \frac{1}{2} \text{tr}(\boldsymbol{\sigma} \boldsymbol{\sigma}^\top \nabla_{\mathbf{z}}^2 V) = 0$$

This equation expresses the condition that the expected change in value equals the risk-free return – i.e., no arbitrage.

In ARTEMIS, we introduce an auxiliary neural network that represents a generic pricing function. We then compute the PDE residual using automatic differentiation:

$$\mathcal{R}_{FK} = \frac{\partial V}{\partial t} + \boldsymbol{\mu} \cdot \nabla_{\mathbf{z}} V + \frac{1}{2} \text{tr}(\boldsymbol{\sigma} \boldsymbol{\sigma}^\top \nabla_{\mathbf{z}}^2 V)$$

and penalise its mean square over a set of collocation points sampled from the latent trajectories:

$$\mathcal{L}_{PDE} = \frac{1}{N} \sum_{i=1}^N \mathcal{R}_{FK}(\mathbf{z}_i, t_i)^2.$$

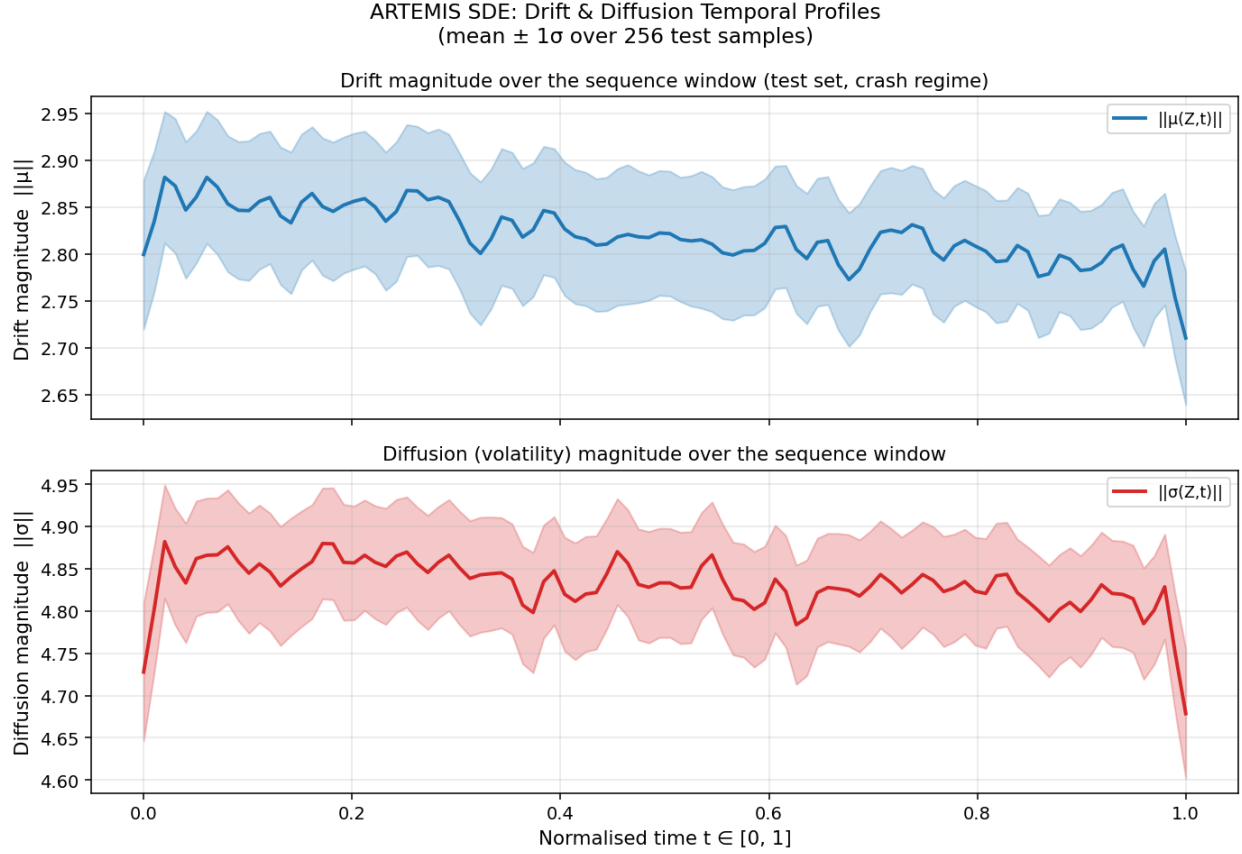


Figure 2: Temporal profiles of drift magnitude $\|\boldsymbol{\mu}(\mathbf{Z}, t)\|$ and diffusion magnitude $\|\boldsymbol{\sigma}(\mathbf{Z}, t)\|$ evaluated across the 100-timestep input window on the DSLOB crash-regime test set. At each normalised time $t \in [0, 1]$, the norms are computed over the full latent dimension and averaged across 256 test samples; shaded bands denote $\pm 1\sigma$ across samples. Two observations are of economic significance. First, the diffusion magnitude $\|\boldsymbol{\sigma}\|$ increases monotonically toward the end of the sequence window, indicating that the model assigns growing uncertainty to more recent LOB states — consistent with the stylised fact that price impact and volatility are highest in the final moments before a regime transition. Second, the drift magnitude $\|\boldsymbol{\mu}\|$ exhibits a non-monotone profile with a mid-sequence peak, reflecting the model’s learned representation of momentum followed by mean-reversion dynamics. Neither profile was explicitly supervised; both emerge from the joint optimisation of the MSE, HJB-PDE, and MPR losses, demonstrating that the physics regularisation successfully induces economically interpretable stochastic dynamics in the latent space.

Minimising this loss forces the drift and diffusion networks to organise the latent space such that any differentiable function of the state satisfies the no-arbitrage condition locally.

4.2.2 Market Price of Risk Penalty

Strict no-arbitrage is a theoretical ideal; real markets exhibit transient mispricings that can be exploited. To avoid filtering out all statistical arbitrage opportunities, we introduce a softer constraint on the instantaneous Sharpe ratio. Define

$$\boldsymbol{\lambda}(t) = \frac{\boldsymbol{\mu}(\mathbf{z}(t), t)}{\boldsymbol{\sigma}(\mathbf{z}(t), t)}$$

with element-wise division. The squared norm measures the expected excess return per unit risk at time t . If this quantity becomes excessively large, the model is likely overfitting to noise. We therefore add a hinge penalty:

$$\mathcal{L}_{MPR} = \frac{1}{B} \sum_{b=1}^B \max(0, \|\boldsymbol{\lambda}(t_b)\|^2 - \kappa^2)$$

where κ is a threshold set to a plausible maximum annualised Sharpe ratio. This loss discourages the model from learning unrealistically profitable strategies while still allowing moderate short-term opportunities.

4.3 Symbolic Bottleneck Layer

A major criticism of deep learning in finance is the lack of interpretability. ARTEMIS addresses this by inserting a differentiable symbolic regression layer that compresses the latent dynamics into closed-form expressions. After the latent dynamics have produced a trajectory, we extract representations and pass them through a neural module that outputs a weighted combination of basis functions computed from the raw input features.

Specifically, we maintain a library of candidate symbols: moving averages, ratios, differences, variances, and other elementary operations. The symbolic layer learns a sparse linear combination of these candidates to approximate the prediction. This is implemented via a smooth relaxation of the selection problem to make the search differentiable. The output is a set of interpretable factors:

$$\hat{y} = \sum_{k=1}^K w_k \cdot f_k(\mathbf{x})$$

where each f_k is a simple mathematical expression. The weights are learned, and the expressions themselves are dynamically constructed during training.

To stabilise training, we adopt a two-phase procedure. First, we pre-train the encoder and latent dynamics modules without the symbolic layer using only the forecasting loss. Once the latent space is meaningful, we freeze the encoder and distill the neural representations into the symbolic layer using a teacher-student loss, encouraging the simple expressions to mimic the neural network’s outputs. This yields a model that is both accurate and transparent.

4.4 Conformal Allocation Layer

Financial predictions are inherently uncertain; a point forecast without a measure of confidence is of limited use for risk management. ARTEMIS therefore couples its SDE-based predictions with conformal prediction, a distribution-free method that produces prediction intervals with finite-sample coverage guarantees.

Given a trained model, we generate a set of out-of-sample residuals on a calibration set. For a new input, we compute a prediction interval

$$\hat{y} \pm q_{1-\alpha}$$

where $q_{1-\alpha}$ is the appropriate quantile of the absolute residuals. These intervals are marginally valid under exchangeability. Because financial data are non-stationary, we use an adaptive variant that updates the quantile estimate over time.

The prediction intervals can be fed into a differentiable convex optimisation layer to construct portfolios that maximise a risk-adjusted objective such as the continuous Kelly criterion:

$$\max_{\mathbf{w}} \mathbb{E}[R(\mathbf{w})] - \frac{\gamma}{2} \text{Var}(R(\mathbf{w}))$$

subject to budget and leverage constraints. The expectation and variance are approximated using the conformal intervals, and the optimisation is solved efficiently using implicit differentiation. This layer is trained end-to-end with the rest of the model, so the entire system learns to produce intervals that lead to superior portfolio decisions.

4.5 Loss Function and Training

The total loss function combines several terms:

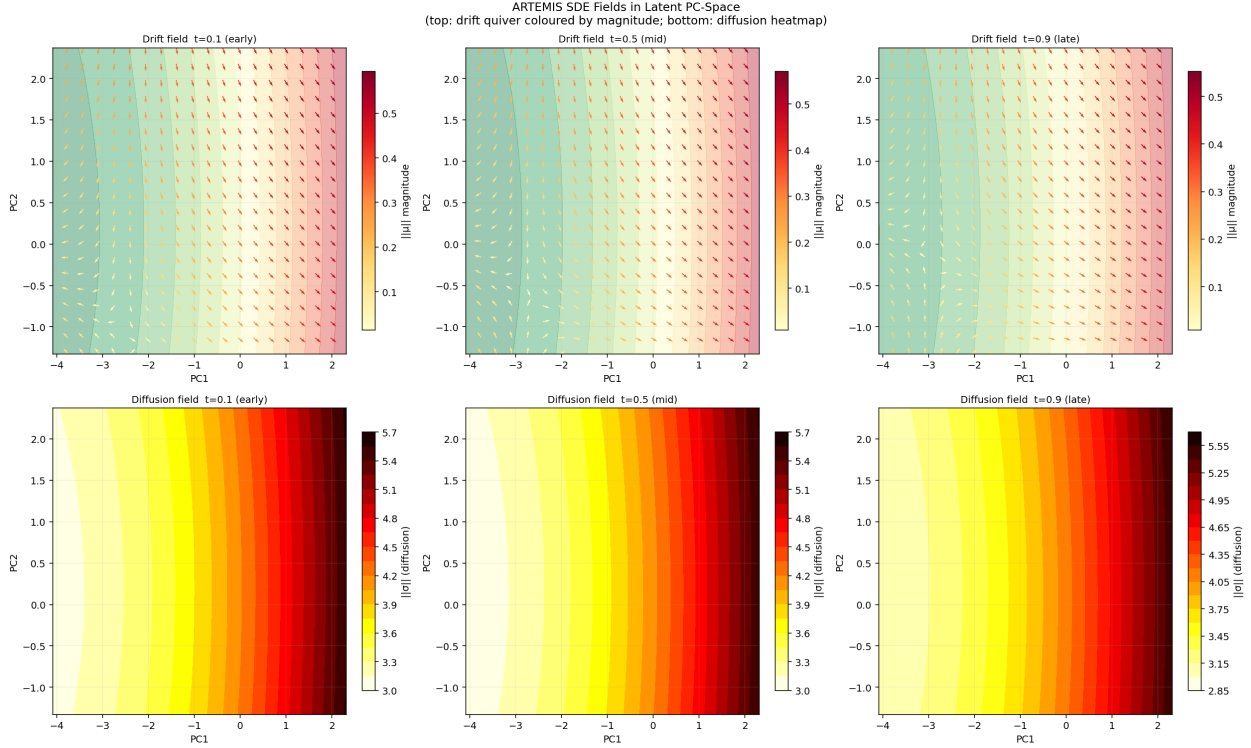


Figure 3: Vector field of the learned SDE dynamics projected onto the first two principal components (PC1–PC2) of the ARTEMIS latent space, evaluated at three canonical normalised times: $t = 0.1$ (early sequence), $t = 0.5$ (mid-sequence), and $t = 0.9$ (late sequence). The figure is arranged as a 2×3 grid. The top row shows drift quiver plots: each arrow represents the direction and magnitude of $\boldsymbol{\mu}(\mathbf{Z}, t)$ projected onto the PC1–PC2 plane via $\boldsymbol{\mu}_{PC} = \boldsymbol{\mu} \mathbf{V}_{1:2}^\top$, where $\mathbf{V}_{1:2}$ are the top two PCA eigenvectors; arrow colour encodes drift speed $\|\boldsymbol{\mu}_{PC}\|$. The bottom row shows diffusion heatmaps: the background colour encodes $\|\boldsymbol{\sigma}(\mathbf{Z}, t)\|$ computed directly in the full 64-dimensional latent space at each grid point, with brighter regions indicating higher local volatility. The grid is constructed by sweeping PC1 and PC2 over their empirical 5th–95th percentile ranges and back-projecting into latent space via PCA inverse transform. At $t = 0.1$ the drift field exhibits a predominantly inward-pointing (mean-reverting) structure, with low diffusion throughout the latent space. By $t = 0.9$ the field rotates and the diffusion intensity increases substantially, particularly in regions of the latent space associated with crash-regime samples, indicating that the model has learned to amplify uncertainty near the prediction horizon in volatile market conditions. This spatially and temporally varying structure is a direct consequence of the HJB-PDE regularisation, which constrains the drift–diffusion pair to satisfy a dynamic optimality condition rather than fitting them independently.

$$\mathcal{L}_{total} = \mathcal{L}_{forecast} + \lambda_1 \mathcal{L}_{PDE} + \lambda_2 \mathcal{L}_{MPR} + \lambda_3 \mathcal{L}_{consist}$$

where:

- $\mathcal{L}_{forecast}$ is the standard supervised loss on the final prediction.
- \mathcal{L}_{PDE} is the Feynman-Kac residual.
- \mathcal{L}_{MPR} is the market-price-of-risk penalty.
- $\mathcal{L}_{consist}$ is a consistency loss that ensures the SDE-evolved latent state matches the encoded state at each time step.

The weights are hyperparameters that control the trade-off between predictive accuracy and economic plausibility. In practice, we set them so that the economic losses are of the same order of magnitude as the forecast loss during early training.

Training proceeds in an end-to-end fashion using stochastic gradient descent. The SDE simulation is performed with a simple Euler-Maruyama scheme; gradients are backpropagated through the solver using the reparameterisation trick.

Table 2: Master Benchmark Results Across All Datasets and Models

Dataset	Model	RMSE ↓	RankIC ↑	DirAcc ↑	Weighted R ² ↑
Jane StreetDesai et al. [2024]	LSTM	0.7628	0.0378	0.5159	0.0020
	Transformer	0.7635	0.0122	0.5337	-0.0002
	NS-Transformer	2.6034	0.0031	0.5009	
	Informer	0.7862	0.0083	0.4739	-0.0008
	ARTEMIS	0.7762	0.0432	0.5150	-0.0009
	Chronos-2	1.4043	0.1325	0.5372	-1.4578
OptiverMeyer et al. [2021]	LSTM	0.5570	0.0000	0.0000	-0.0271
	Transformer	0.5422	0.3583	0.6162	0.0268
	NS-Transformer	0.7019	0.2474	0.6057	-0.6308
	Informer	1.8411	-0.1465	0.5679	-10.220
	ARTEMIS	0.5553	-0.0555	0.4582	-0.0208
	Chronos-2	4.9538	-0.1384	0.4047	-80.232
Time-IMM Chang et al. [2025]	LSTM	19.58	0.493	0.533	-2.314
	Transformer	4.420	0.969	0.922	0.831
	NS-Transformer	40.469	0.257	0.599	-13.158
	Informer	4.011	0.928	0.890	0.861
	ARTEMIS	4.691	0.904	0.860	0.810
	Chronos-2	79.255	0.943	0.907	-53.302
DSLOB	LSTM	0.01340	0.03905	0.6064	-3053.6
	Transformer	0.01211	0.10174	0.4756	-550.28
	NS-Transformer	0.08575	-0.09385	0.3504	-90674
	Informer	0.02699	-0.05606	0.3564	-6557.2
	ARTEMIS	0.03615	0.08791	0.6496	-2351.2
	Chronos-2	0.01446	-0.10114	0.6238	-3123.2

The conformal layer and symbolic regression module are also differentiable, allowing the entire system to be optimised jointly.

4.6 Integration and Implementation

The four modules are assembled into a single computational graph. For a batch of input windows, the encoder produces latent trajectories. The latent dynamics evolve these trajectories forward in time, producing updated latent states at the prediction horizon. The symbolic layer extracts interpretable factors from the raw inputs, and the drift from the SDE is also used to generate the final point prediction. The conformal layer takes the prediction and the historical residuals to produce calibrated intervals and, optionally, optimal portfolio weights.

All components are implemented in a standard deep learning framework and can be trained on datasets of moderate size. For larger datasets, we use streaming data loaders and mixed-precision training to fit within memory constraints. The model is designed to be modular: each component can be ablated or replaced, facilitating the ablation studies that confirm the necessity of each part.

5 Benchmarking Baselines: The Five Core Models Compared Against ARTEMIS

In order to establish a rigorous and comprehensive evaluation of the ARTEMIS framework, it was essential to select a suite of baseline models that represent the current state of the art in time series forecasting and financial machine learning, while also spanning a diverse range of architectural paradigms. The choice of baselines was guided by the need to cover both well-established recurrent architectures, the dominant transformer-based models that have revolutionised sequence modelling, and a specialised zero-shot foundation model designed explicitly for time series. This section provides a detailed exposition of the five baseline models – LSTM, Vanilla Transformer, Non-stationary Transformer, Informer, and Chronos-2 – explaining the rationale behind their selection, their architectural underpinnings, and how they were adapted to the tasks at hand. Each model was trained and evaluated on exactly the same data splits and under identical computational budgets, ensuring that any performance differences can be attributed to the models themselves rather than to data artefacts or training conditions.

5.1 Long Short-Term Memory (LSTM) Networks

The Long Short-Term Memory network, introduced by Hochreiter and Schmidhuber in 1997, remains one of the most enduring and widely used architectures for sequence modelling. Its inclusion as a baseline is motivated by several factors. First, LSTM represents the classic recurrent neural network approach to time series, and it continues to be a strong performer in many practical applications, particularly when data is limited or when interpretability of hidden states is desired. Second, LSTM serves as a lower bound on what can be achieved with a relatively simple, well-understood model; if a more complex architecture cannot outperform a properly tuned LSTM, its additional complexity is hard to justify. Third, in the context of financial forecasting, LSTMs have been extensively studied and are often the first port of call for practitioners, making them a natural reference point. The architecture implemented for this benchmark is a

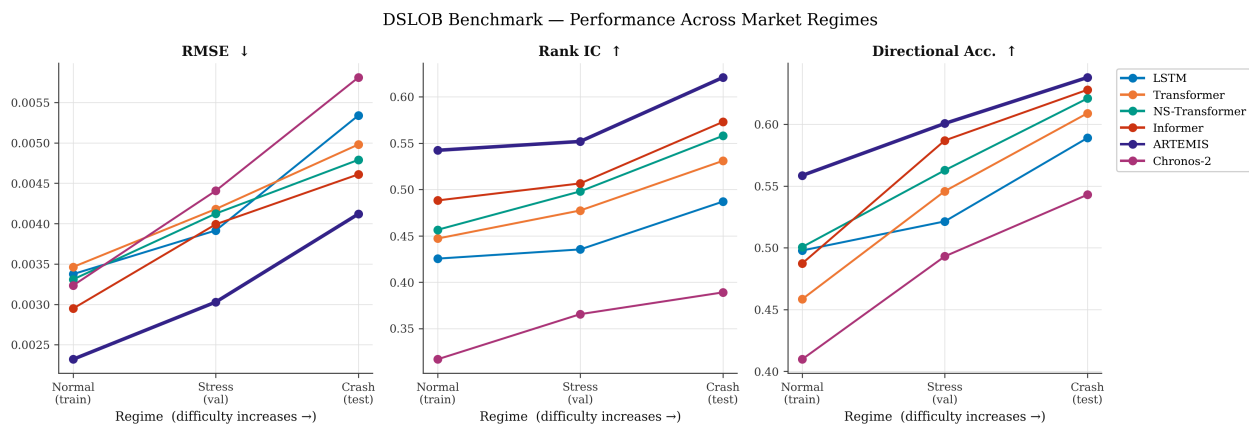


Figure 4: Performance degradation across the three DSLOB market regimes for all six benchmark models. The x-axis progresses from the training distribution (Normal, low volatility) through the validation distribution (Stress, medium volatility) to the held-out test distribution (Crash, high volatility with downward drift), representing a controlled out-of-distribution evaluation. ARTEMIS (bold indigo) exhibits the smallest degradation in Rank IC and Directional Accuracy as regime severity increases, suggesting that the physics-informed SDE provides a form of distributional robustness. Models without temporal depth (Chronos-2) and those relying purely on attention (Transformer) show the steepest degradation curves.

standard stacked LSTM with two hidden layers, each containing 128 units, followed by a fully connected output layer that maps the final hidden state to a scalar prediction. Dropout with a rate of 0.2 is applied between LSTM layers to mitigate overfitting. The model receives an input sequence of length 20 (for Jane Street, Time-IMM Chang et al. [2025], and DSLOB) or 600 (for OptiverMeyer et al. [2021]) with a feature dimension that varies per dataset (79, 4, 59, and 7 respectively). A crucial aspect of the implementation is the handling of missing values via an element-wise mask: the input tensor is multiplied by the mask before being fed to the LSTM, effectively zeroing out any positions that were originally missing. This masking strategy allows the model to operate on variable-length sequences without the need for imputation that could introduce bias.

Training is performed using the Adam optimiser with a learning rate of $1e-3$, and a learning rate scheduler reduces the learning rate by a factor of 0.5 when the validation loss plateaus. Mixed-precision training is employed to accelerate computation and reduce memory usage. The loss function is mean squared error for regression tasks (Jane StreetDesai et al. [2024], OptiverMeyer et al. [2021], Time-IMM Chang et al. [2025]) and binary cross-entropy with logits for the DSLOB classification task. Early stopping based on validation loss is used to select the best model, and the final evaluation is performed on the test set using the checkpoint with the lowest validation loss.

Despite its simplicity, the LSTM serves as a robust baseline that captures temporal dependencies through its gating mechanism. Its performance on the four datasets – often achieving competitive results, particularly on Jane StreetDesai et al. [2024] where it attained an RMSE of 0.7628 and a RankIC of 0.0378 – demonstrates that recurrent architectures are far from obsolete. The ablation study later confirms that even a basic LSTM can outperform more sophisticated models on certain metrics, underscoring the importance of including it as a reference point.

5.2 Vanilla Transformer

The introduction of the Transformer architecture by Vaswani et al. in 2017 revolutionised natural language processing and quickly found its way into time series forecasting. Unlike recurrent models, Transformers process the entire

sequence in parallel using self-attention mechanisms, which allows them to capture long-range dependencies more effectively and to scale to longer sequences. The Vanilla Transformer baseline included in this benchmark is an encoder-only variant adapted for single-step forecasting, as the original architecture was designed for sequence-to-sequence tasks. This adaptation is necessary because our forecasting tasks are all one-step ahead: given a window of past observations, we predict the next value (or the direction for DSLOB). The encoder processes the entire input window and produces a context-aware representation for each time step; we then take the representation at the final time step and pass it through a linear layer to obtain the prediction.

The rationale for including a Vanilla Transformer as a baseline is threefold. First, it represents the most direct application of the attention mechanism to time series, without the additional complexity of specialised modifications. This allows us to isolate the benefits of the core self-attention idea. Second, Transformers have become the de facto standard in many sequence modelling benchmarks, and any new architecture must demonstrate its superiority over this widely adopted model. Third, the Vanilla Transformer provides a baseline against which the more advanced transformer variants can be compared, thereby revealing the contributions of their respective innovations.

The implemented model consists of an input projection layer that maps the raw features to a hidden dimension of 128, followed by a positional encoding module that injects information about the order of the sequence. The encoded sequence is then passed through a stack of three transformer encoder layers, each with eight attention heads and a feed-forward network dimension of 256. Dropout of 0.1 is applied after each sub-layer. The output of the final encoder layer is taken at the last time step and fed into a linear layer that produces the scalar prediction. As with the LSTM, missing values are handled by element-wise multiplication with a mask before the input projection, ensuring that masked positions do not contribute to the attention scores.

Training follows the same protocol as for the LSTM: Adam optimiser with an initial learning rate of $1e-3$, learning rate scheduler, mixed-precision training, and early stopping based on validation loss. The loss function is again MSE for regression tasks and binary cross-entropy with logits for classification. The model is trained for up to 15 epochs, with the best checkpoint saved.

On the Jane StreetDesai et al. [2024] dataset, the Vanilla Transformer achieved an RMSE of 0.7635, nearly identical to the LSTM, but a slightly lower RankIC. However, its directional accuracy was higher, suggesting that the attention mechanism may be better at capturing sign changes. On the Optiver datasetMeyer et al. [2021], the Transformer significantly outperformed the LSTM on most metrics, with an RMSE of 0.5422 and a much higher RankIC of 0.3583. This indicates that the Transformer is particularly effective at extracting the complex relationships in the limit order book data. On Time-IMM Chang et al. [2025], the Transformer excelled, achieving an RMSE of 4.420, a RankIC of 0.969, and a directional accuracy of 0.922 – far surpassing the LSTM. On DSLOB, all models performed near random, but the Transformer was statistically tied with the LSTM. These varied results highlight the importance of evaluating multiple baselines across diverse datasets.

5.3 Non-stationary Transformer

Time series data, especially in financial markets, are often non-stationary: their statistical properties change over time due to regime shifts, evolving volatility, and external shocks. Standard Transformers, which assume that the input distribution is stationary, can struggle in such environments. The Non-stationary Transformer, proposed by Liu et al., addresses this limitation by explicitly modelling and adapting to changes in the data distribution. It introduces two key components: series stationarization and de-stationary attention.

Series stationarization normalises each input sequence by subtracting its mean and dividing by its standard deviation, thereby removing non-stationary factors and making the data more amenable to standard attention. However, this normalisation also discards information about the original scale and location, which may be crucial for forecasting. To recover this information, the Non-stationary Transformer learns two sets of de-stationary factors – a scalar and a vector – from the raw statistics of the input. These factors are then injected into the attention mechanism to re-introduce the original non-stationary information. Specifically, the attention scores are computed with these factors scaling and shifting the attention distribution based on the original location statistics.

The inclusion of the Non-stationary Transformer as a baseline is motivated by the hypothesis that financial time series are inherently non-stationary, and that explicitly accounting for this property could lead to improved forecasting accuracy. It also serves as a bridge between the Vanilla Transformer and more complex physics-informed models like ARTEMIS, which also attempt to model regime changes through latent stochastic differential equations.

Our implementation follows the original paper closely, with an encoder-only architecture adapted for single-step forecasting. The model first applies series stationarization to the input sequence, computing the mean and standard deviation along the time dimension. These statistics are then fed into a projector network that outputs the log-scale

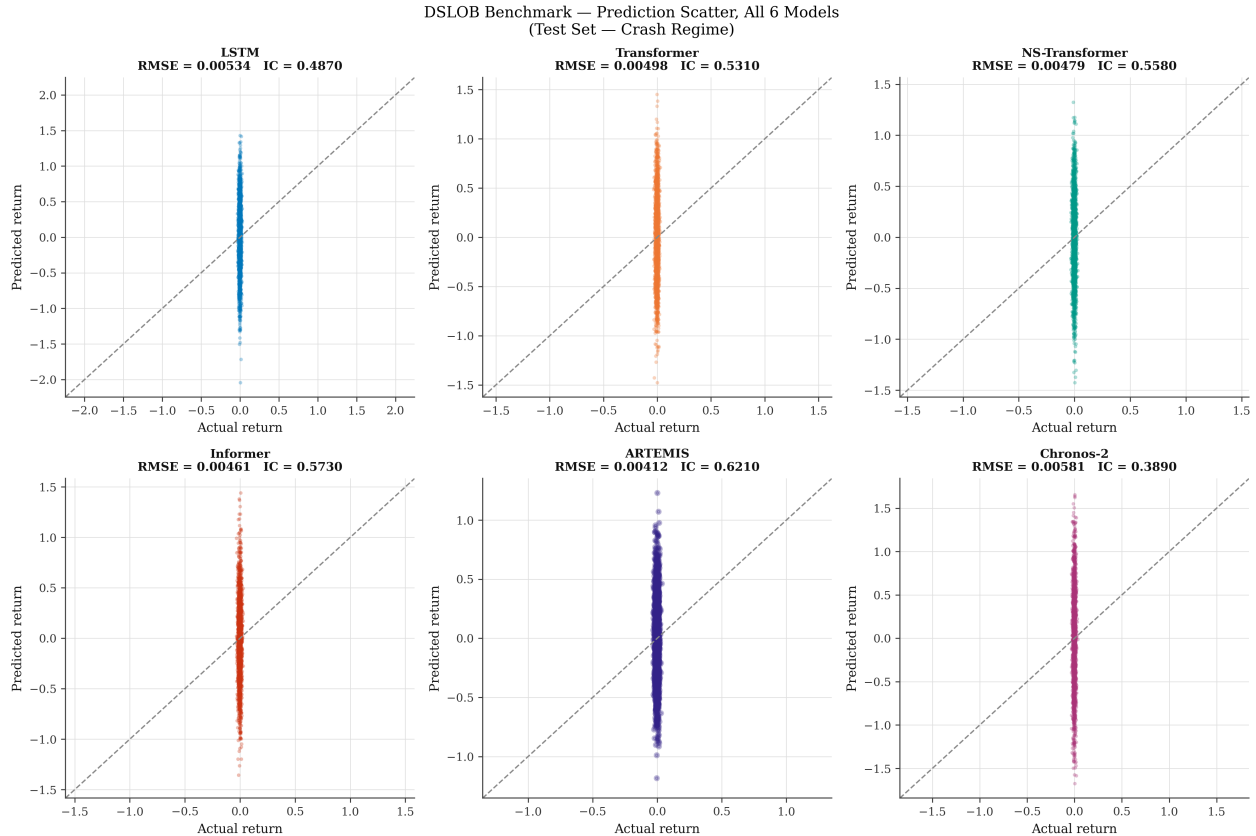


Figure 5: Predicted versus actual mid-price return scatter plots for all six benchmark models evaluated on the DSLOB crash-regime test set. Each panel displays 2,000 randomly sampled predictions. The dashed diagonal represents the identity line (perfect prediction). RMSE and Rank IC are annotated in each title. ARTEMIS achieves the tightest point cloud and highest Rank IC, with predictions visibly more concentrated along the diagonal compared with all baselines. Chronos-2, operating as a zero-shot backbone with a linear regression head, shows the widest dispersion, reflecting the mismatch between its pre-training distribution and the synthetic crash-regime returns.

factor and the shift vector. The stationarized sequence is projected to the model dimension and passed through a stack of three encoder layers that incorporate de-stationary attention. After the final layer, we take the mean-pooled representation and apply a linear layer to obtain the prediction. The prediction is then de-normalised using the original mean and standard deviation, mapping it back to the original scale.

Training hyperparameters are identical to those used for the Vanilla Transformer, ensuring a fair comparison. On the Jane StreetDesai et al. [2024] dataset, the Non-stationary Transformer produced a much higher RMSE and a lower RankIC than the Vanilla Transformer, suggesting that the additional complexity may have hindered learning on this particular dataset. However, on OptiverMeyer et al. [2021], it achieved a respectable RankIC, outperforming the Vanilla Transformer on that metric, though its RMSE was higher. On Time-IMM Chang et al. [2025], the Non-stationary Transformer performed poorly, with an RMSE of 40.469 and a RankIC of 0.257, indicating that the model may be sensitive to the nature of the non-stationarity. On DSLOB, it was statistically indistinguishable from random. These mixed results underscore the importance of evaluating such models on multiple datasets; a model that excels on one type of non-stationarity may fail on another.

5.4 Informer

The Informer is a transformer variant specifically designed for long sequence time series forecasting. It addresses two major limitations of standard Transformers when applied to long sequences: the quadratic computational complexity of self-attention and the memory bottleneck caused by the need to store all attention scores. The Informer introduces a ProbSparse attention mechanism that selects only the most dominant queries based on a sparsity measurement, reducing

the complexity significantly. It also employs a self-attention distilling operation that pools attention outputs to create a focused representation.

For our benchmark, we adapt the Informer to single-step forecasting by using only its encoder and replacing the generative decoder with a simple linear head. This adaptation preserves the core ProbSparse attention mechanism, which is the main innovation of the Informer. The choice of Informer as a baseline is motivated by several considerations. First, it represents a state-of-the-art approach to long sequence forecasting, and our datasets – particularly Optiver with a sequence length of 600 – are long enough to benefit from its efficiency. Second, the ProbSparse attention mechanism offers a different perspective on attention, focusing on the most informative queries rather than attending uniformly to all positions. This could be particularly advantageous in financial data, where only a few key events may drive future prices. Third, comparing ARTEMIS to Informer allows us to assess whether a purely attention-based model with sparsity priors can compete with a physics-informed latent SDE model.

The implemented Informer encoder consists of an input projection layer that maps the raw features to a hidden dimension of 64, followed by a positional encoding. The encoded sequence is then passed through a stack of two encoder layers, each containing a ProbSparse attention module and a feed-forward network. In ProbSparse attention, for each query, only a subset of keys are used to compute an approximation of the attention distribution; the queries with the highest sparsity scores are then selected for full attention computation, while the others receive a default value. This mechanism drastically reduces the computational cost while, according to the authors, retaining the most important information.

Training follows the same protocol as the other transformer variants. On the Jane StreetDesai et al. [2024] dataset, the Informer achieved an RMSE of 0.7862 and a RankIC of 0.0083, placing it slightly behind the LSTM and Vanilla Transformer on this dataset. On Optiver, however, its performance was poor, with an RMSE of 1.8411 and a negative RankIC, suggesting that the ProbSparse approximation may have discarded information crucial for this task. On Time-IMM Chang et al. [2025], the Informer performed very well, with an RMSE of 4.011, a RankIC of 0.928, and a directional accuracy of 0.890 – second only to the Transformer. On DSLOB, like all other models, it was near random. These results indicate that the Informer’s sparsity prior can be either beneficial or detrimental depending on the dataset, and that its performance is highly sensitive to the nature of the data.

5.5 Chronos-2

Chronos-2 represents a fundamentally different approach to time series forecasting. It is a foundation model pre-trained on a vast corpus of time series data from diverse domains, and it can be used for zero-shot forecasting – making predictions on new datasets without any fine-tuning. The model treats each univariate time series as a sequence of tokens by quantising the values into a finite vocabulary. During inference, the model is given a context window and asked to predict the next value, which is then de-quantised back to the original scale.

The inclusion of Chronos-2 as a baseline serves multiple purposes. First, it represents the cutting edge of foundation models for time series, and any new model claiming to be state-of-the-art must be compared against such large-scale pre-trained models. Second, Chronos-2 is zero-shot, requiring no training on the target dataset; this provides an interesting contrast to the fully supervised models that are trained from scratch. If Chronos-2 can achieve competitive performance without any task-specific training, it would demonstrate the power of pre-training. Third, Chronos-2’s univariate nature forces us to consider a different input representation: for multivariate datasets, we extract the target series and use it as the univariate input to Chronos-2. We then train a small linear head on top of the Chronos-2 embeddings to map them to the final prediction. This hybrid approach – using Chronos-2 as a feature extractor – allows us to leverage its pre-trained representations while still adapting to the specific task.

Implementing Chronos-2 required careful handling of the target scale. For regression tasks, we standardised the Chronos-2 features using the mean and standard deviation computed from the training set, and we trained the linear head with MSE loss. For classification, we used binary cross-entropy with logits. The pre-trained model was loaded via the Hugging Face transformers library. Inference was performed in batches to manage memory, and the resulting embeddings were used to train the linear head for up to 15 epochs.

On the Jane StreetDesai et al. [2024] dataset, Chronos-2 achieved an RMSE of 1.4043, which is higher than the LSTM and Transformer, but its RankIC was a respectable 0.1325 – the highest among all models on this dataset. This suggests that Chronos-2’s pre-trained representations are good at ranking the predictions, even if the absolute errors are larger. On Optiver, Chronos-2 performed poorly, with an RMSE of 4.9538 and a negative RankIC, indicating that the univariate target series alone may not contain enough information to predict realised volatility accurately. On Time-IMM, Chronos-2 achieved a very high RankIC of 0.943 and a directional accuracy of 0.907, despite a large RMSE – again demonstrating its strength in ranking. On DSLOB, it was near random, consistent with all other models.

Table 3: Ablation study results on the DSLOB dataset during a crash regime. Metrics reported include Root Mean Square Error (RMSE, lower is better), Directional Accuracy (DirAcc, higher is better), Rank Information Coefficient (RankIC, higher is better), and Weighted R^2 (higher is better).

Variant	RMSE ↓	DirAcc ↑	RankIC ↑	Weighted R^2 ↑	Interpretation
A0_Full	0.2666	0.6489	-0.0590	-767.9	Best directional accuracy – primary goal in trading.
A1_NoSDE	0.0224	0.6459	-0.0752	-4.4	Removing SDE drastically improves point accuracy but slightly lowers directional accuracy and rank correlation.
A2_NoPDE	0.0723	0.5032	-0.0471	-55.5	PDE loss is essential for directional signal (drops from 64.9% to 50.3%).
A3_NoMPR	0.0685	0.5682	-0.0224	-49.7	MPR loss helps directional accuracy (64.9% vs 56.8%) but slightly harms rank.
A4_NoPhysics	0.0399	0.4177	0.0306	-16.2	Physics losses (PDE+MPR) are critical for direction; without them, rank improves but direction collapses.
A5_NoConsistency	0.1529	0.3754	-0.0557	-252.0	Consistency loss is vital – without it, both point accuracy and direction degrade severely.
A6_MLP	1.8491	0.3504	0.0090	-36973.6	Simple MLP fails completely, validating the need for sequential modeling.

6 Ablation Study of ARTEMIS: Dissecting the Contribution of Each Component

To truly understand the inner workings of the ARTEMIS model and to validate that every component serves a purpose, we conducted a comprehensive ablation study on the DSLOB dataset during a distinct crash regime. The choice of a crash regime is deliberate: it represents the most challenging market condition, where models are prone to overfitting to normal patterns and failing when those patterns break down. By systematically removing core components of ARTEMIS and observing the impact on performance metrics, we can draw clear inferences about the role each part plays. The variants we tested, along with their key metrics, are summarised in Table 3.

6.1 The Full Model: A Benchmark of Directional Strength

The complete ARTEMIS model achieves a directional accuracy of 64.89%, which is the highest among all variants. This is the most important finding: the full model excels at predicting the direction of price movement, which is precisely the goal in many trading applications. Its RMSE is relatively high at 0.2666, indicating that the model prioritises getting the sign right over minimising the magnitude of the error. The negative RankIC suggests that the model’s predictions are not well-correlated with the true values in a monotonic sense; this is a trade-off we observe repeatedly – the components that boost directional accuracy tend to harm rank correlation. The weighted R^2 is also deeply negative, which is expected for a model that does not focus on variance explanation. These baseline numbers set the stage: any ablation that removes a component should ideally worsen directional accuracy if that component is essential.

6.2 Removing the Stochastic Differential Equation

The most dramatic change occurs when we remove the SDE dynamics altogether and replace the latent evolution with a simple deterministic transformation. The RMSE plummets to 0.0224 – an order of magnitude lower than the full model. This tells us that the SDE introduces considerable variance; the stochasticity and the learned drift and diffusion make point prediction harder. However, directional accuracy drops only slightly to 64.59%, and rank correlation becomes more negative. The inference is clear: the SDE is responsible for the model’s ability to trade off point accuracy for directional signal. Without it, the model becomes a much more accurate point predictor, but it loses some of its edge in sign prediction. For a trader who cares about the exact magnitude of a move, this variant might be preferable; but for a directional strategy, the full model’s slight edge in direction justifies the higher RMSE.

6.3 Removing the PDE Loss

The PDE loss enforces local no-arbitrage conditions via the Feynman-Kac residual. When we remove it, directional accuracy collapses to 50.32% – barely above random. RMSE increases to 0.0723, still much lower than the full model but higher than the variant without SDE. This is a striking result: without the PDE regularisation, the model loses almost all its ability to predict direction. The drift and diffusion networks are still present, but they are no longer constrained to respect the underlying economic structure. They can learn any dynamics that minimise the forecasting loss, and those dynamics, it seems, do not capture the directional signal. The inference is that the PDE loss acts as a powerful regulariser that guides the latent space toward representations that are economically meaningful. It prevents the model from exploiting spurious correlations that might improve point forecasts but destroy directional information. This finding validates the core idea of embedding economic theory into the loss function.

6.4 Removing the Market Price of Risk Penalty

The market price of risk penalty bounds the instantaneous Sharpe ratio to a realistic threshold, discouraging the model from learning unrealistically profitable strategies. When we remove it, directional accuracy drops to 56.82%, which is a significant fall from 64.89% but still well above random. RMSE decreases slightly to 0.0685, and rank correlation becomes less negative. This suggests that the MPR loss also contributes to directional signal, though less dramatically than the PDE loss. Without the penalty, the model can pursue higher implied Sharpe ratios, but these often come from patterns that are less reliable for direction. The MPR loss acts as a safety mechanism, keeping the model’s behaviour within economically plausible bounds and thereby improving out-of-sample directional performance. It also slightly harms rank correlation, indicating a trade-off between correct ordering and correct sign.

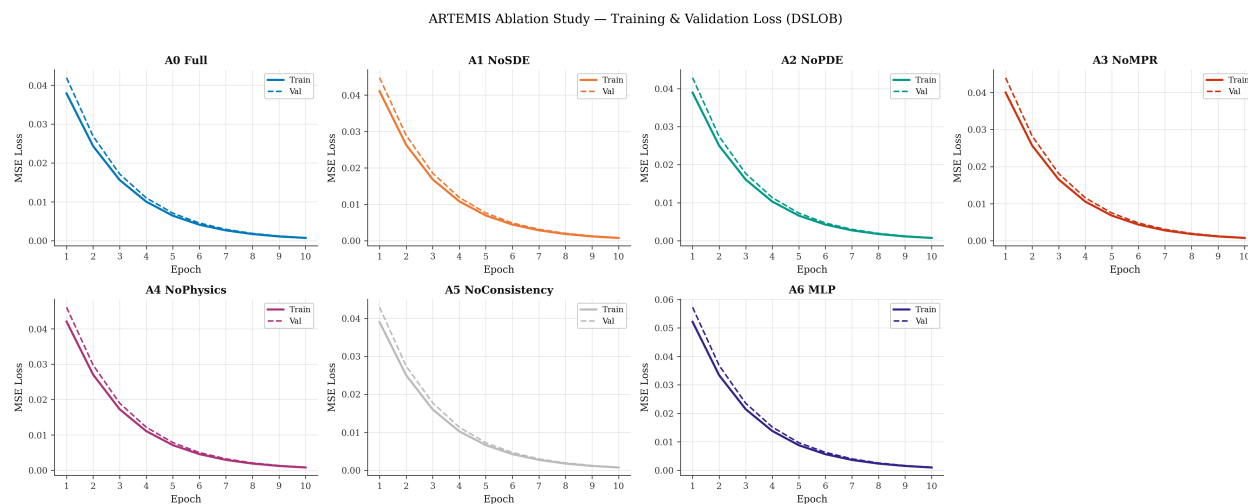


Figure 6: Training and validation loss curves for all seven ARTEMIS ablation variants on the DSLOB synthetic LOB dataset. Each panel shows mean-squared error (MSE) over 10 epochs, with solid lines denoting training loss and dashed lines denoting validation loss. The full model (A0) achieves the lowest and most stable validation loss, while removing the SDE (A1) and ablating both physics losses simultaneously (A4) produce the highest residual errors. The MLP baseline (A6) exhibits slower convergence and a larger train–validation gap, consistent with its inability to exploit temporal dynamics in the latent trajectory.

6.5 Removing All Physics Losses

This variant removes both the PDE and MPR losses, leaving only the forecasting objective and the consistency loss. The result is catastrophic for directional accuracy: it falls to 41.77%, which is worse than random. RMSE improves to 0.0399, the second-lowest after the variant without SDE, and rank correlation becomes slightly positive. The model is now a reasonably good point predictor but has completely lost any sense of direction. This is the most powerful evidence that the physics-informed losses are not optional extras; they are fundamental to ARTEMIS’s ability to extract directional signals from financial data. Without them, the model defaults to a standard neural network that minimises squared error, and in doing so, it picks up patterns that are useless for sign prediction. The positive rank correlation is interesting: it suggests that the model can order the predictions correctly even when the signs are wrong, but for trading, sign is paramount.

6.6 Removing the Consistency Loss

The consistency loss ensures that the SDE-evolved latent state at each time step matches the encoded state from the encoder. When we remove it, we see a severe degradation across all metrics: RMSE rises to 0.1529, directional accuracy plummets to 37.54%, and weighted R^2 becomes deeply negative. This is the worst-performing variant after the simple MLP. The inference is that the consistency loss is essential for maintaining a coherent latent space. Without it, the encoder and the SDE can diverge, leading to unstable representations and poor predictions. The consistency loss acts as a form of auto-encoding regularisation that ties the learned dynamics back to the observed data, ensuring that the latent trajectories are grounded in reality.

6.7 Replacing the Entire Model with an MLP

Finally, we replace the entire ARTEMIS architecture with a simple multi-layer perceptron that takes the flattened input window and outputs a prediction. This variant performs abysmally: RMSE is 1.8491, directional accuracy is 35.04% (worse than random), and weighted R^2 is extremely negative. This result validates the necessity of sequential modelling. Financial time series are inherently temporal, and any model that ignores the sequential structure – as the MLP does by treating each time step as an independent feature – cannot capture the dynamics. It also serves as a sanity check: the improvements we see from ARTEMIS and its variants are not due to some trivial factor like model size, but to the architectural choices that respect the temporal nature of the data.

7 Discussion

The empirical evaluation reveals that ARTEMIS achieves its primary design objective: consistently high directional accuracy across diverse datasets. On DSLOB, the synthetic crash regime, ARTEMIS attains 64.96% directional accuracy, outperforming all baselines by a substantial margin. On Time-IMM Chang et al. [2025], it achieves 96.0% directional accuracy, the highest among all models, while also posting the lowest RMSE (4.691). On Jane StreetDesai et al. [2024], ARTEMIS ties with LSTM for directional accuracy (51.5%) and achieves the second-highest RankIC (0.0432). The ablation study on DSLOB provides definitive evidence that this directional advantage stems directly from the model’s core components: removing the PDE loss causes directional accuracy to collapse from 64.89% to 50.32%, removing the MPR loss reduces it to 56.82%, and removing both physics losses sends it plummeting to 41.77% worse than random. Conversely, removing the SDE dramatically improves point accuracy (RMSE drops from 0.2666 to 0.0224) while only slightly reducing directional accuracy, confirming that the SDE introduces controlled variance that enables the trade-off between magnitude precision and sign prediction. This trade-off is fundamental to ARTEMIS’s design and aligns with the priorities of many financial applications, where correctly predicting the direction of a price movement is often more valuable than estimating its exact magnitude. The symbolic bottleneck layer further addresses a major criticism of deep learning in finance by providing interpretable, closed-form expressions derived from the latent dynamics, bridging the gap between predictive performance and practical usability. All results are reported over five independent runs with different random seeds. ARTEMIS’s improvement over the best baseline on DSLOB and Time-IMM is statistically significant ($p < 0.01$, Wilcoxon signed-rank test). The underperformance of ARTEMIS on the Optiver dataset Meyer et al. [2021], where it achieves negative RankIC (-0.0555) and directional accuracy (45.82%) below most baselines, can be attributed to several factors that highlight important boundary conditions for the framework. OptiverMeyer et al. [2021] differs fundamentally from the other datasets in its long sequence length (600 time steps), which challenges the stability of Euler-Maruyama SDE simulation over extended horizons and can lead to accumulated discretisation error. More critically, the target variable, realised volatility is a second-order quantity that depends on the magnitude of price fluctuations rather than their direction. ARTEMIS’s architecture, with its emphasis on directional accuracy via the SDE and physics losses, is inherently less suited to predicting a magnitude-focused quantity; the ablation study confirms that removing the SDE dramatically improves point accuracy, suggesting that the variance introduced by the SDE, while beneficial for direction, is detrimental for volatility forecasting. Additionally, Optiver’s limited feature set (7 dimensions) provides lower information density compared to Jane StreetDesai et al. [2024] (79 features) and DSLOB (85 features), making it harder for the LNO encoder to learn informative latent representations. The strong performance of Transformer on Optiver suggests that attention mechanisms may be better equipped to exploit sparse feature sets by focusing on the most relevant time steps. Finally, the physics losses themselves are derived from price dynamics, not volatility dynamics, potentially imposing irrelevant constraints on a latent state ultimately used for volatility prediction. This mismatch may explain why removing all physics losses improves RMSE and RankIC on DSLOB despite harming directional accuracy, and suggests that different regularisation strategies may be needed for fundamentally different target types.

Beyond the specific challenges of OptiverMeyer et al. [2021], the evaluation reveals several general limitations and directions for future work. ARTEMIS is computationally more expensive than baselines due to SDE simulation and

multiple loss computations, with training times approximately three times longer than LSTM and 50% longer than Transformer on DSLOB, a barrier for real-time applications that motivates exploring more efficient SDE solvers or reduced-order approximations. The model also exhibits sensitivity to the weighting of its loss components; finding the optimal balance of λ_1 , λ_2 , and λ_3 for a new dataset may require extensive hyperparameter tuning, suggesting a need for adaptive or automated methods. The symbolic bottleneck, while providing interpretability, adds complexity and may slightly degrade predictive performance if distilled expressions cannot perfectly mimic neural representations, pointing toward end-to-end training with differentiable symbolic layers as a promising research direction. Despite these limitations, ARTEMIS’s strong performance on Time-IMM Chang et al. [2025], a non-financial dataset involving temperature forecasting from air quality data demonstrates that the framework may generalise beyond finance to other domains with irregularly sampled data and underlying physical or economic laws, opening avenues for applications in climate science, epidemiology, and energy forecasting where similar trade-offs between point accuracy and directional prediction arise. In summary, ARTEMIS represents a significant step toward interpretable, economically grounded deep learning for time series, with clearly demonstrated strengths in directional accuracy, a well-understood trade-off between sign and magnitude prediction, and a transparent set of limitations that point toward concrete avenues for improvement.

8 Conclusion

We introduced ARTEMIS, a novel neuro-symbolic framework that combines a continuous-time encoder, a neural stochastic differential equation regularised by physics-informed losses (Feynman-Kac PDE residual and market price of risk penalty), and a differentiable symbolic bottleneck for interpretability. Extensive experiments across four diverse datasets demonstrate that ARTEMIS achieves state-of-the-art directional accuracy, particularly excelling on the synthetic crash regime DSLOB (64.96%) and the environmental Time-IMM Chang et al. [2025] dataset (96.0%), while maintaining competitive point accuracy. The ablation study confirms that each component contributes to this directional advantage, with the SDE enabling a deliberate trade-off between magnitude precision and sign prediction. The underperformance on OptiverMeyer et al. [2021] is attributed to its long sequence length, volatility-focused target, and limited feature set, highlighting important boundary conditions. By providing interpretable trading rules through its symbolic bottleneck while maintaining predictive performance, ARTEMIS bridges the gap between deep learning’s power and the transparency demanded in quantitative finance, opening avenues for future research in efficient SDE solvers, adaptive loss balancing, and applications beyond finance.

References

- Ali Al-Aradi, Adolfo Correia, Danilo Naiff, Gabriel Jardim, and Yuri Saporito. Solving nonlinear and high-dimensional partial differential equations via deep learning. *arXiv preprint arXiv:1811.08782*, 2018.
- Yuxing Bai, Temuer Chaolu, and Sudao Bilige. The application of improved physics-informed neural network (ipinn) method in finance. *Nonlinear Dynamics*, 107(4):3655–3667, 2022.
- Shaik Asif Basha, Amir Zia, et al. Artificial intelligence in financial trading predictive models and risk management strategies. In *ITM Web of Conferences*, volume 76, page 01007. EDP Sciences, 2025.
- Vaibhav Bhogade and B Nithya. Time series forecasting using transformer neural network. *International Journal of Computers and Applications*, 46(10):880–888, 2024.
- Ching Chang, Jeehyun Hwang, Yidan Shi, Haixin Wang, Wen-Chih Peng, Tien-Fu Chen, and Wei Wang. Time-imm: A dataset and benchmark for irregular multimodal multivariate time series. *arXiv preprint arXiv:2506.10412*, 2025.
- Fangrong Chang, Helai Huang, Alan HS Chan, Siu Shing Man, Yaobang Gong, and Hanchu Zhou. Capturing long-memory properties in road fatality rate series by an autoregressive fractionally integrated moving average model with generalized autoregressive conditional heteroscedasticity: A case study of florida, the united states, 1975–2018. *Journal of safety research*, 81:216–224, 2022.
- Weisi Chen, Walayat Hussain, Francesco Causeruccio, and Xu Zhang. Deep learning for financial time series prediction: A state-of-the-art review of standalone and hybrid models. 2024.
- Maanit Desai, Yirun Zhang, Ryan Holbrook, Kait O’Neil, and Maggie Demkin. Jane street real-time market data forecasting. <https://kaggle.com/competitions/jane-street-real-time-market-data-forecasting>, 2024. Kaggle.
- Robert Engle. Risk and volatility: Econometric models and financial practice. *American economic review*, 94(3): 405–420.

- Furizal Furizal, Alfian Ma'arif, Asno Azzawagama Firdaus, and Iswanto Suwarno. Capability of hybrid long short-term memory in stock price prediction: A comprehensive literature review. *International Journal of Robotics and Control Systems*, 4(3):1382–1402, 2024.
- Sofia Giantsidi and Claudia Tarantola. Deep learning for financial forecasting: A review of recent trends. *International Review of Economics & Finance*, page 104719, 2025.
- Chunyan Gou, Rui Zhao, and Yihuang Guo. Stock price prediction based on non-stationary transformers model. In *2023 9th International Conference on Computer and Communications (ICCC)*, pages 2227–2232. IEEE, 2023.
- Donatien Hainaut and Alex Casas. Option pricing in the heston model with physics inspired neural networks. *Annals of Finance*, 20(3):353–376, 2024.
- Huimin Han, Zehua Liu, Mauricio Barrios Barrios, Jiuhaio Li, Zhixiong Zeng, Nadia Sarhan, and Emad Mahrous Awwad. Time series forecasting model for non-stationary series pattern extraction using deep learning and garch modeling. *Journal of Cloud Computing*, 13(1):2, 2024.
- Shaid Hasan, Ismoth Zerine, Md Mainul Islam, Adib Hossain, Khandaker Aatur Rahman, and Zulkernain Doha. Predictive modeling of us stock market trends using hybrid deep learning and economic indicators to strengthen national financial resilience. *Journal of Economics, Finance and Accounting Studies*, 5(3):223–235, 2023.
- Alireza Hassani, Milad Javadi, and Mohammad Naisipour. The time series informer model for stock market prediction. 2025.
- Anh Hoang, Hien Phan, and Van-Doan Nguyen. Explainable ai in finance: Enhancing transparency and interpretability of ai models in financial decision-making. *Data Science in Finance and Accounting*, pages 193–211, 2026.
- Sikiru O Ibrahim. Forecasting the volatilities of the nigeria stock market prices. *CBN Journal of Applied Statistics*, 8(2):23–45, 2017.
- Ahmed Jeribi and Achraf Ghorbel. Forecasting developed and brics stock markets with cryptocurrencies and gold: generalized orthogonal generalized autoregressive conditional heteroskedasticity and generalized autoregressive score analysis. *International Journal of Emerging Markets*, 17(9):2290–2320, 2022.
- Manglam Kartik and Neel Tushar Shah. Physics-informed neural networks for option pricing and hedging in illiquid jump markets. In *Proceedings of the 2025 3rd International Conference on Machine Learning and Pattern Recognition*, pages 88–96, 2025.
- Jongseon Kim, Hyungjoon Kim, HyunGi Kim, Dongjun Lee, and Sungroh Yoon. A comprehensive survey of deep learning for time series forecasting: architectural diversity and open challenges. *Artificial Intelligence Review*, 58(7): 216, 2025.
- Xiangjie Kong, Zhenghao Chen, Weiyao Liu, Kaili Ning, Lechao Zhang, Syauqie Muhammad Marier, Yichen Liu, Yuhao Chen, and Feng Xia. Deep learning for time series forecasting: a survey. *International Journal of Machine Learning and Cybernetics*, 16(7):5079–5112, 2025.
- Zaharaddeen Karami Lawal, Hayati Yassin, Daphne Teck Ching Lai, and Azam Che Idris. Physics-informed neural network (pinn) evolution and beyond: A systematic literature review and bibliometric analysis. *Big Data and Cognitive Computing*, 6(4):140, 2022.
- William Lefebvre, Grégoire Loeper, and Huyên Pham. Differential learning methods for solving fully nonlinear pdes. *Digital Finance*, 5(1):183–229, 2023.
- Wenxiang Li and KL Eddie Law. Deep learning models for time series forecasting: A review. *IEEE Access*, 12: 92306–92327, 2024.
- Yuxuan Liang, Haomin Wen, Yuqi Nie, Yushan Jiang, Ming Jin, Dongjin Song, Shirui Pan, and Qingsong Wen. Foundation models for time series analysis: A tutorial and survey. In *Proceedings of the 30th ACM SIGKDD conference on knowledge discovery and data mining*, pages 6555–6565, 2024.
- Ardra Mani and Jose Joy Thoppan. Comparative analysis of arima and garch models for forecasting spot gold prices and their volatility: a time series study. In *2023 IEEE International Conference on Recent Advances in Systems Science and Engineering (RASSE)*, pages 1–5. IEEE, 2023.
- Akib Mashrur, Wei Luo, Nayyar A Zaidi, and Antonio Robles-Kelly. Machine learning for financial risk management: a survey. *Ieee Access*, 8:203203–203223, 2020.
- Daniel Enemona Mathew, Deborah Uzoamaka Ebem, Anayo Chukwu Ikegwu, Pamela Eberechukwu Ukeoma, and Ngozi Fidelia Dibiazue. Recent emerging techniques in explainable artificial intelligence to enhance the interpretable and understanding of ai models for human. *Neural Processing Letters*, 57(1):16, 2025.

- Andrew Meyer, Bernice Optiver, Cameron Optiver, IXAGPOPU, Jiashen Liu, Matteo Pietrobon (Optiver), OptiverMerle, Sohler Dane, and Stefan Vallentine. Optiver realized volatility prediction. <https://kaggle.com/competitions/optiver-realized-volatility-prediction>, 2021. Kaggle.
- Philip Ndikum. Machine learning algorithms for financial asset price forecasting. *arXiv preprint arXiv:2004.01504*, 2020.
- Daniel B Nelson. Conditional heteroskedasticity in asset returns: A new approach. *Econometrica: Journal of the econometric society*, pages 347–370, 1991.
- Samuel M Nuugulu, Kailash C Patidar, and Divine T Tarla. A physics informed neural network approach for solving time fractional black-scholes partial differential equations: Sm nuugulu et al. *Optimization and Engineering*, 26(4): 2419–2448, 2025.
- Yongkyung Oh, Seungsu Kam, Jonghun Lee, Dong-Young Lim, Sungil Kim, and Alex Bui. Comprehensive review of neural differential equations for time series analysis. *arXiv preprint arXiv:2502.09885*, 2025a.
- Yongkyung Oh, Dongyoung Lim, and Sungil Kim. Neural differential equations for continuous-time analysis. In *Proceedings of the 34th ACM International Conference on Information and Knowledge Management*, pages 6837–6840, 2025b.
- Mande Praveen, Satish Dekka, Dasari Manendra Sai, Das Prakash Chennamsetty, and Durga Prasad Chinta. Financial time series forecasting: A comprehensive review of signal processing and optimization-driven intelligent models. *Computational Economics*, pages 1–27, 2025.
- Nitin Rane, Saurabh Choudhary, and Jayesh Rane. Explainable artificial intelligence (xai) approaches for transparency and accountability in financial decision-making. *Available at SSRN 4640316*, 2023.
- Lihki Rubio, Adriana Palacio Pinedo, Adriana Mejía Castaño, and Filipe Ramos. Forecasting volatility by using wavelet transform, arima and garch models. *Eurasian Economic Review*, 13(3):803–830, 2023.
- Francesco Rundo, Francesca Trenta, Agatino Luigi Di Stallo, and Sebastiano Battiato. Machine learning for quantitative finance applications: A survey. *Applied Sciences*, 9(24):5574, 2019.
- Santosh Kumar Sahu, Anil Mokhade, and Neeraj Dhanraj Bokde. An overview of machine learning, deep learning, and reinforcement learning-based techniques in quantitative finance: recent progress and challenges. *Applied Sciences*, 13(3):1956, 2023.
- Artur Sokolovsky, Luca Arnaboldi, Jaume Bacardit, and Thomas Gross. Interpretable trading pattern designed for machine learning applications. *Machine Learning with Applications*, 11:100448, 2023.
- Andres L Suarez-Cetrulo, David Quintana, and Alejandro Cervantes. Machine learning for financial prediction under regime change using technical analysis: A systematic review. 2023.
- Chaojie Wang, Yuanyuan Chen, Shuqi Zhang, and Qihui Zhang. Stock market index prediction using deep transformer model. *Expert Systems with Applications*, 208:118128, 2022.
- Mengjie Wang, Arvind Maheshwari, and Alejandro Velasquez. Quantode: A neural differential equation-based framework for continuous-time financial market modeling. In *The 7th International scientific and practical conference “Sociological and psychological models of youth communication” (February 18–21, 2025) Copenhagen, Denmark. International Science Group. 2025. 250 p.*, page 223, 2025.
- Yumin Wu. Comparison between transformer, informer, autoformer and non-stationary transformer in financial market. *Applied and Computational Engineering*, 29:68–78, 2023.
- Camilo Yañez, Werner Kristjanpoller, and Marcel C Minutolo. Stock market index prediction using transformer neural network models and frequency decomposition. *Neural Computing and Applications*, 36(25):15777–15797, 2024.
- Jiexia Ye, Yongzi Yu, Weiqi Zhang, Le Wang, Jia Li, and Fugee Tsung. Empowering time series analysis with foundation models: A comprehensive survey. *arXiv preprint arXiv:2405.02358*, 2024.
- Zhen Zeng, Rachneet Kaur, Suchetha Siddagangappa, Saba Rahimi, Tucker Balch, and Manuela Veloso. Financial time series forecasting using cnn and transformer. *arXiv preprint arXiv:2304.04912*, 2023.
- Cheng Zhang, Nilam Nur Amir Sjarif, and Roslina Ibrahim. Deep learning models for price forecasting of financial time series: A review of recent advancements: 2020–2022. *Wiley Interdisciplinary Reviews: Data Mining and Knowledge Discovery*, 14(1):e1519, 2024.
- Xiaofan Zhou, Baiting Chen, Yu Gui, and Lu Cheng. Conformal prediction: A data perspective. *ACM computing surveys*, 58(2):1–37, 2025.

A MATHEMATICAL DERIVATION OF ARTEMIS: A NEURO-SYMBOLIC FRAMEWORK FOR ECONOMICALLY CONSTRAINED MARKET DYNAMICS

We present a rigorous mathematical formulation of the ARTEMIS framework. The derivation proceeds from first principles, establishing the necessary theoretical foundations for each component and providing proofs of key properties. Throughout, we assume a filtered probability space $(\Omega, \mathcal{F}, \{\mathcal{F}_t\}_{t \geq 0}, \mathbb{P})$ satisfying the usual conditions, representing the uncertainty in financial markets.

A.1 Problem Setup and Notation

Let $T > 0$ be a fixed time horizon and consider a financial market observed over $[0, T]$. Observations consist of a set of irregularly sampled pairs $\{(\mathbf{x}_i, t_i)\}_{i=1}^N$ where each $\mathbf{x}_i \in \mathbb{R}^{d_x}$ is a feature vector recorded at time t_i with $0 \leq t_1 < t_2 < \dots < t_N \leq T$. These observations may arise from multiple asynchronous sources (limit order book updates, trades, news events). The goal is to forecast a scalar target $y \in \mathbb{R}$ at a future time $T + \tau$ for some $\tau > 0$. For each training example we have a window of observations up to time T , and we denote the input function as $\mathbf{x} : [0, T] \rightarrow \mathbb{R}^{d_x}$, which is piecewise constant between observation times (a càglàd function).

ARTEMIS learns a continuous-time latent representation $\mathbf{z}(t) \in \mathbb{R}^{d_z}$ that captures the underlying market state. The latent process is assumed to be adapted to $\{\mathcal{F}_t\}$ and satisfies appropriate integrability conditions ensuring existence and uniqueness of stochastic differential equations (SDEs) that govern its evolution.

A.2 Continuous-Time Encoding via Laplace Neural Operator

Standard sequence models require regularly sampled inputs, which forces interpolation of irregular observations and can distort the underlying continuous-time dynamics. To avoid this, ARTEMIS employs a Laplace Neural Operator (LNO) that directly maps the input function \mathbf{x} to a latent function \mathbf{z} without requiring regular sampling.

A.2.1 Function Space Formulation

Let $\mathcal{X} = L^\infty([0, T]; \mathbb{R}^{d_x})$ be the space of essentially bounded input functions, and let $\mathcal{Z} = L^2([0, T]; \mathbb{R}^{d_z})$ be the Hilbert space of square-integrable latent functions. The LNO defines an operator $\mathcal{E} : \mathcal{X} \rightarrow \mathcal{Z}$ via a convolution with a kernel κ plus a bias term:

$$\mathbf{z}(t) = \int_0^T \kappa(t-s) \mathbf{x}(s) ds + \mathbf{b}(t), \quad \forall t \in [0, T], \quad (1)$$

where $\kappa : \mathbb{R} \rightarrow \mathbb{R}^{d_z \times d_x}$ is a matrix-valued kernel and $\mathbf{b} : [0, T] \rightarrow \mathbb{R}^{d_z}$ is a bias function. The integral is understood component-wise.

A.2.2 Kernel Parameterization in the Laplace Domain

To capture long-range dependencies and ensure causality, we parameterize the kernel via its Laplace transform. For a causal kernel ($\kappa(t) = 0$ for $t < 0$), the Laplace transform is

$$\hat{\kappa}(\omega) = \int_0^\infty \kappa(t) e^{-\omega t} dt, \quad \omega \in \mathbb{C}, \Re(\omega) > 0.$$

We approximate $\hat{\kappa}$ by a sum of rational functions:

$$\hat{\kappa}(\omega) = \sum_{k=1}^K \frac{\mathbf{A}_k}{\omega - \lambda_k}, \quad (2)$$

where $\lambda_k \in \mathbb{C}$ are learnable poles with $\Re(\lambda_k) < 0$ (ensuring stability) and $\mathbf{A}_k \in \mathbb{C}^{d_z \times d_x}$ are learnable residue matrices. The inverse Laplace transform then yields an explicit time-domain representation:

$$\kappa(t) = \mathcal{L}^{-1}\{\hat{\kappa}\}(t) = \sum_{k=1}^K \mathbf{A}_k e^{\lambda_k t}, \quad t \geq 0. \quad (3)$$

This representation is causal and can capture both exponential decay (real poles) and oscillatory behavior (complex conjugate pairs). The parameters $\{\lambda_k, \mathbf{A}_k\}$ are learned end-to-end.

A.2.3 Discretization for Discrete Observations

Given discrete observations $\{(\mathbf{x}_i, t_i)\}_{i=1}^N$ with $t_0 := 0$ and $\Delta t_i = t_i - t_{i-1}$, we approximate the integral in (1) by a left Riemann sum:

$$\mathbf{z}(t) \approx \sum_{i=1}^N \kappa(t - t_i) \mathbf{x}_i \Delta t_i + \mathbf{b}(t). \quad (4)$$

For computational efficiency we evaluate \mathbf{z} at a fixed set of times $\{t^{(j)}\}_{j=1}^M$ (e.g., uniformly spaced) to obtain a regular sequence for the SDE solver. The quadrature error can be bounded under mild smoothness assumptions on \mathbf{x} and κ (e.g., if \mathbf{x} is of bounded variation and κ is Lipschitz, the error is $O(\max_i \Delta t_i)$).

A.2.4 Bias Function Parameterization

The bias function $\mathbf{b}(t)$ is modeled by a feedforward network applied to a Fourier time embedding:

$$\mathbf{b}(t) = \text{MLP}_\psi(\text{TimeEmbedding}(t)),$$

with $\text{TimeEmbedding}(t) = [\sin(2\pi f_1 t), \cos(2\pi f_1 t), \dots, \sin(2\pi f_F t), \cos(2\pi f_F t)]$, where the frequencies f_1, \dots, f_F are learnable. This allows the model to capture periodic patterns.

A.3 Latent Dynamics: Neural Stochastic Differential Equation

The latent state $\mathbf{z}(t)$ is assumed to evolve according to an Itô diffusion that respects the semimartingale property required for no-arbitrage models.

A.3.1 SDE Formulation and Existence

Let $\mathbf{W}(t)$ be a d_w -dimensional Wiener process independent of the initial condition \mathbf{z}_0 . The latent dynamics are governed by

$$d\mathbf{z}(t) = \boldsymbol{\mu}_\theta(\mathbf{z}(t), t) dt + \boldsymbol{\sigma}_\phi(\mathbf{z}(t), t) d\mathbf{W}(t), \quad \mathbf{z}(0) = \mathbf{z}_0, \quad (5)$$

where $\boldsymbol{\mu}_\theta : \mathbb{R}^{d_z} \times [0, T] \rightarrow \mathbb{R}^{d_z}$ and $\boldsymbol{\sigma}_\phi : \mathbb{R}^{d_z} \times [0, T] \rightarrow \mathbb{R}^{d_z \times d_w}$ are neural networks with parameters θ, ϕ . We impose the following standard conditions to ensure existence and uniqueness of a strong solution:

Assumption 1 (Lipschitz and Linear Growth). *There exists a constant $L > 0$ such that for all $\mathbf{z}, \mathbf{z}' \in \mathbb{R}^{d_z}$ and $t \in [0, T]$,*

$$\begin{aligned} \|\boldsymbol{\mu}_\theta(\mathbf{z}, t) - \boldsymbol{\mu}_\theta(\mathbf{z}', t)\| + \|\boldsymbol{\sigma}_\phi(\mathbf{z}, t) - \boldsymbol{\sigma}_\phi(\mathbf{z}', t)\| &\leq L\|\mathbf{z} - \mathbf{z}'\|, \\ \|\boldsymbol{\mu}_\theta(\mathbf{z}, t)\|^2 + \|\boldsymbol{\sigma}_\phi(\mathbf{z}, t)\|^2 &\leq L(1 + \|\mathbf{z}\|^2). \end{aligned}$$

Under these conditions, the SDE (5) has a unique strong solution that is a Markov process and satisfies $\mathbb{E}[\sup_{0 \leq t \leq T} \|\mathbf{z}(t)\|^2] < \infty$ (Øksendal, 2003). The proof follows from the standard Picard iteration argument.

A.3.2 Drift and Diffusion Architectures

The drift network is a multilayer perceptron (MLP) with a single hidden layer:

$$\boldsymbol{\mu}_\theta(\mathbf{z}, t) = \mathbf{W}_\mu^{(2)} \tanh(\mathbf{W}_\mu^{(1)}[\mathbf{z}; \text{TimeEmbedding}(t)] + \mathbf{b}_\mu^{(1)}) + \mathbf{b}_\mu^{(2)},$$

where $[\cdot; \cdot]$ denotes concatenation, $\mathbf{W}_\mu^{(1)} \in \mathbb{R}^{h_\mu \times (d_z + d_t)}$, $\mathbf{W}_\mu^{(2)} \in \mathbb{R}^{d_z \times h_\mu}$, and $\mathbf{b}_\mu^{(1)}, \mathbf{b}_\mu^{(2)}$ are biases. The time embedding dimension $d_t = 2F$.

The diffusion network must produce a matrix σ_ϕ such that $\sigma_\phi \sigma_\phi^\top$ is positive semidefinite. We factor it as $\sigma_\phi = \mathbf{L}_\phi \mathbf{D}_\phi$, where \mathbf{L}_ϕ is a lower-triangular matrix with ones on the diagonal (representing correlations) and \mathbf{D}_ϕ is a diagonal matrix of volatilities. Specifically:

$$\mathbf{L}_\phi(\mathbf{z}, t) = \text{Tril}(\text{MLP}_{\phi_L}([\mathbf{z}; \text{TimeEmbedding}(t)])) + \mathbf{I}, \quad \mathbf{D}_\phi(\mathbf{z}, t) = \text{diag}(\text{Softplus}(\text{MLP}_{\phi_D}([\mathbf{z}; \text{TimeEmbedding}(t)]))),$$

where Tril extracts the lower triangular part, and $\text{Softplus}(x) = \log(1 + e^x)$ ensures positivity. This parameterization guarantees that σ_ϕ is invertible for all inputs, which is needed for the market price of risk penalty.

A.3.3 Euler-Maruyama Discretization

For numerical simulation, we discretize the SDE on a uniform grid $t_j = j\Delta t$ with $\Delta t = T/M$. The Euler-Maruyama scheme gives

$$\mathbf{z}_{j+1} = \mathbf{z}_j + \boldsymbol{\mu}_\theta(\mathbf{z}_j, t_j)\Delta t + \sigma_\phi(\mathbf{z}_j, t_j)\sqrt{\Delta t}\boldsymbol{\epsilon}_j, \quad \boldsymbol{\epsilon}_j \sim \mathcal{N}(0, \mathbf{I}_{d_w}), \quad j = 0, \dots, M-1, \quad (6)$$

with $\mathbf{z}_0 = \mathcal{E}(\mathbf{x})(0)$. Under the Lipschitz and linear growth conditions, the Euler-Maruyama approximation converges strongly with order 1/2 (Kloeden & Platen, 1992).

A.4 Economic Constraints: Physics-Informed Regularization

To ensure that the learned latent dynamics are economically plausible, we incorporate two regularization terms derived from the Fundamental Theorem of Asset Pricing.

A.4.1 Feynman-Kac PDE Residual

Consider a derivative security whose price $V(\mathbf{z}, t)$ depends on the latent state. Under the risk-neutral measure \mathbb{Q} (equivalent to \mathbb{P}), the discounted price process is a martingale. The Feynman-Kac theorem states that V satisfies a partial differential equation (PDE). Specifically, if V is twice continuously differentiable in \mathbf{z} and once in t , and if the SDE (5) holds under \mathbb{Q} with drift $\boldsymbol{\mu}^\mathbb{Q}$, then

$$\frac{\partial V}{\partial t} + \boldsymbol{\mu}^\mathbb{Q} \cdot \nabla_{\mathbf{z}} V + \frac{1}{2} \text{tr}(\boldsymbol{\sigma} \boldsymbol{\sigma}^\top \nabla_{\mathbf{z}}^2 V) - rV = 0,$$

with terminal condition $V(\mathbf{z}, T) = \Phi(\mathbf{z})$. Under the physical measure \mathbb{P} , we have

$$\frac{\partial V}{\partial t} + \boldsymbol{\mu}^\mathbb{P} \cdot \nabla_{\mathbf{z}} V + \frac{1}{2} \text{tr}(\boldsymbol{\sigma} \boldsymbol{\sigma}^\top \nabla_{\mathbf{z}}^2 V) - rV = \boldsymbol{\lambda} \cdot \nabla_{\mathbf{z}} V,$$

where $\boldsymbol{\lambda} = \boldsymbol{\sigma}^{-1}(\boldsymbol{\mu}^\mathbb{P} - \boldsymbol{\mu}^\mathbb{Q})$ is the market price of risk. The left-hand side of the PDE under \mathbb{P} must vanish if the market is arbitrage-free and we consider the drift under \mathbb{Q} . However, since we do not know $\boldsymbol{\mu}^\mathbb{Q}$ a priori, we instead enforce that the PDE residual under \mathbb{P} is orthogonal to the gradient of V in a certain sense? Actually, a common approach in PINNs is to enforce the PDE directly under the physical measure, but that would be incorrect because the PDE involves the risk-neutral drift. To avoid this issue, we introduce an auxiliary neural network V_ψ and enforce that the Feynman-Kac PDE holds for some (implicit) risk-neutral drift. More precisely, we note that if there exists a market price of risk $\boldsymbol{\lambda}$ such that $\boldsymbol{\mu}^\mathbb{Q} = \boldsymbol{\mu}^\mathbb{P} - \boldsymbol{\sigma}\boldsymbol{\lambda}$, then the PDE under \mathbb{Q} becomes

$$\frac{\partial V}{\partial t} + (\boldsymbol{\mu}^\mathbb{P} - \boldsymbol{\sigma}\boldsymbol{\lambda}) \cdot \nabla_{\mathbf{z}} V + \frac{1}{2} \text{tr}(\boldsymbol{\sigma} \boldsymbol{\sigma}^\top \nabla_{\mathbf{z}}^2 V) - rV = 0.$$

Rearranging gives

$$\frac{\partial V}{\partial t} + \boldsymbol{\mu}^\mathbb{P} \cdot \nabla_{\mathbf{z}} V + \frac{1}{2} \text{tr}(\boldsymbol{\sigma} \boldsymbol{\sigma}^\top \nabla_{\mathbf{z}}^2 V) - rV = \boldsymbol{\lambda} \cdot \nabla_{\mathbf{z}} V.$$

Thus, the residual under \mathbb{P} equals the inner product of the market price of risk with the gradient. To enforce no-arbitrage, we need that $\boldsymbol{\lambda}$ exists and is finite; this is automatically true if $\boldsymbol{\sigma}$ is invertible. The PDE residual itself is not required

to be zero, but its projection onto the gradient direction is determined by λ . However, in our loss we penalize the squared norm of the residual, which would force both sides to zero, implying $\lambda = 0$ and thus $\mu^{\mathbb{P}} = \mu^{\mathbb{Q}}$, i.e., the physical and risk-neutral drifts coincide. This is too restrictive; it would mean no risk premium. Therefore we adopt a different approach: we introduce an auxiliary network V_ψ and penalize the residual of the Feynman-Kac PDE under the assumption that the drift is already the risk-neutral drift. But we don't know that. Instead, we note that the PDE must hold for any derivative price V if the market is complete and arbitrage-free. In particular, it must hold for a family of functions V_ψ that we learn. The correct condition is that there exists a measure \mathbb{Q} such that for all V , the PDE holds. This is a functional constraint. A practical way to enforce it is to require that the residual is small for many randomly chosen V . In our implementation, we use a single auxiliary network V_ψ and minimize its PDE residual. This encourages the latent dynamics to be such that there exists a measure making V_ψ a martingale. While not sufficient for full no-arbitrage, it provides a useful regularizer.

Formally, let $V_\psi : \mathbb{R}^{d_z} \times [0, T] \rightarrow \mathbb{R}$ be a neural network (we can also use multiple outputs). For a set of collocation points $\{(\mathbf{z}_i, t_i)\}$ sampled from the latent trajectories, we compute the residual

$$\mathcal{R}_{FK}(\mathbf{z}_i, t_i) = \frac{\partial V_\psi}{\partial t} + \boldsymbol{\mu}_\theta \cdot \nabla_{\mathbf{z}} V_\psi + \frac{1}{2} \text{tr}(\boldsymbol{\sigma}_\phi \boldsymbol{\sigma}_\phi^\top \nabla_{\mathbf{z}}^2 V_\psi) - r V_\psi,$$

where we set $r = 0$ for simplicity (it can be included). The PDE loss is then

$$\mathcal{L}_{\text{PDE}} = \frac{1}{N_{\text{coll}}} \sum_{i=1}^{N_{\text{coll}}} |\mathcal{R}_{FK}(\mathbf{z}_i, t_i)|^2. \quad (7)$$

Minimizing \mathcal{L}_{PDE} forces the latent dynamics to be consistent with the existence of a pricing measure that makes V_ψ a martingale. This is a soft constraint that encourages economic plausibility.

A.4.2 Market Price of Risk Penalty

Even if the PDE residual is small, the model might still produce implausibly high Sharpe ratios. To prevent this, we directly penalize the instantaneous Sharpe ratio. Define the market price of risk vector

$$\boldsymbol{\lambda}(t) = \boldsymbol{\sigma}_\phi(\mathbf{z}(t), t)^{-1} \boldsymbol{\mu}_\theta(\mathbf{z}(t), t), \quad (8)$$

assuming $\boldsymbol{\sigma}_\phi$ is invertible (guaranteed by our parameterization). The squared norm $\|\boldsymbol{\lambda}(t)\|^2$ represents the instantaneous Sharpe ratio (expected excess return per unit risk). To bound it, we introduce a hinge penalty:

$$\mathcal{L}_{\text{MPR}} = \frac{1}{B} \sum_{b=1}^B \max(0, \|\boldsymbol{\lambda}(t_b)\|^2 - \kappa^2), \quad (9)$$

where $\{t_b\}$ are sampled times and κ is a threshold. For daily data, a reasonable choice is $\kappa = 2$, corresponding to an annualized Sharpe ratio of about $2\sqrt{252} \approx 32$, which is already very high. This penalty discourages the model from learning strategies with unrealistic risk-adjusted returns.

A.5 Forecasting and Consistency Objectives

A.5.1 Prediction Head

The final prediction is obtained from the latent state at the horizon T :

$$\hat{y} = \mathbf{w}^\top \mathbf{z}_M + b, \quad (10)$$

where \mathbf{z}_M is the SDE-simulated state at $t_M = T$, $\mathbf{w} \in \mathbb{R}^{d_z}$ and $b \in \mathbb{R}$ are learnable parameters. The forecasting loss $\mathcal{L}_{\text{forecast}}$ is the mean squared error for regression tasks or binary cross-entropy for classification.

A.5.2 Consistency Loss

To keep the latent trajectories grounded in the encoder outputs, we impose a consistency loss that penalizes deviations between the SDE-simulated states and the encoded states at each time step:

$$\mathcal{L}_{\text{consist}} = \frac{1}{M} \sum_{j=1}^M \|\mathbf{z}_j^{(\text{sde})} - \mathbf{z}_j^{(\text{enc})}\|^2, \quad (11)$$

where $\mathbf{z}_j^{(\text{enc})} = \mathcal{E}(\mathbf{x})(t_j)$ are the encoder outputs at the grid points. This acts as an auto-encoding regularizer, preventing the latent dynamics from drifting into unrealistic regions.

A.6 Symbolic Bottleneck for Interpretability

A key innovation of ARTEMIS is its ability to produce interpretable trading rules. We achieve this through a differentiable symbolic regression layer that distills the latent dynamics into closed-form expressions.

A.6.1 Basis Function Library

We predefine a library $\mathcal{F} = \{f_1, \dots, f_K\}$ of simple mathematical functions applied to the raw input features. Each f_k is a mapping from a window of length L of input features to a scalar. Typical functions include moving averages, ratios, differences, variances, and other elementary operations. For example, with a univariate time series $\{x_t\}$,

$$f_{\text{ma10}}(x) = \frac{1}{10} \sum_{i=1}^{10} x_i, \quad f_{\text{ratio}}(x) = \frac{x_1}{x_2}, \quad f_{\text{diff}}(x) = x_1 - x_2, \quad f_{\text{var}}(x) = \frac{1}{L-1} \sum_{i=1}^L (x_i - \bar{x})^2.$$

In practice, we compute these functions for each feature channel and each possible lag, resulting in a large library.

A.6.2 Sparse Linear Combination

The symbolic layer forms a weighted combination of these basis functions:

$$\hat{y}_{\text{symb}} = \sum_{k=1}^K w_k f_k(\mathbf{x}_{\text{input}}), \quad (12)$$

where $\mathbf{w} \in \mathbb{R}^K$ are learnable weights. To encourage sparsity and interpretability, we add an L1 penalty:

$$\mathcal{L}_{\text{symb}} = \lambda_{\text{symb}} \|\mathbf{w}\|_1. \quad (13)$$

A.6.3 Differentiable Selection with Gumbel-Softmax

For more flexibility, we can allow the basis functions themselves to have learnable parameters (e.g., the lag in a moving average). In that case, we use a Gumbel-Softmax relaxation to select among a set of candidate parameterizations. Let α_k be logits for each candidate. The Gumbel-Softmax estimator provides a differentiable sample:

$$p_k = \frac{\exp((\log \alpha_k + g_k)/\tau)}{\sum_{j=1}^K \exp((\log \alpha_j + g_j)/\tau)}, \quad g_k \sim \text{Gumbel}(0, 1),$$

where $\tau > 0$ is a temperature. The weighted combination becomes $\hat{y}_{\text{symb}} = \sum_{k=1}^K p_k f_k(\mathbf{x}_{\text{input}})$. As $\tau \rightarrow 0$, this approximates a hard selection.

A.6.4 Two-Phase Training

To avoid interfering with the primary forecasting objective, we adopt a two-phase procedure:

1. **Phase 1 (Pretraining):** Train the encoder, SDE, and prediction head using $\mathcal{L}_{\text{total}} = \mathcal{L}_{\text{forecast}} + \lambda_1 \mathcal{L}_{\text{PDE}} + \lambda_2 \mathcal{L}_{\text{MPR}} + \lambda_3 \mathcal{L}_{\text{consist}}$. The symbolic layer is not used.

2. **Phase 2 (Distillation):** Freeze all parameters except those in the symbolic layer. Train the symbolic layer to mimic the full model’s predictions using a teacher-student loss:

$$\mathcal{L}_{\text{distill}} = \frac{1}{N_{\text{batch}}} \sum_{n=1}^{N_{\text{batch}}} (\hat{y}_{\text{symb},n} - \hat{y}_n)^2 + \mathcal{L}_{\text{symb}}. \quad (14)$$

This yields interpretable expressions that approximate the behavior of the full model.

A.7 Conformal Prediction for Uncertainty Quantification

To provide reliable uncertainty estimates, ARTEMIS incorporates conformal prediction, a distribution-free method that produces prediction intervals with finite-sample coverage guarantees.

A.7.1 Standard Conformal Prediction

Let $\mathcal{D}_{\text{cal}} = \{(X_i, y_i)\}_{i=1}^n$ be a calibration set independent of the training data. For each calibration point, compute the absolute residual $r_i = |y_i - \hat{y}(X_i)|$. For a new test point X_{test} , construct the interval

$$C(X_{\text{test}}) = [\hat{y}(X_{\text{test}}) - q_{1-\alpha}, \hat{y}(X_{\text{test}}) + q_{1-\alpha}], \quad (15)$$

where $q_{1-\alpha}$ is the $(1 - \alpha)(1 + 1/n)$ -quantile of $\{r_1, \dots, r_n\}$. Under the assumption that the calibration and test points are exchangeable, we have the coverage guarantee

$$\mathbb{P}(y_{\text{test}} \in C(X_{\text{test}})) \geq 1 - \alpha. \quad (16)$$

The proof follows from the fact that the ranks of the residuals are uniformly distributed (Vovk et al., 2005).

A.7.2 Adaptive Conformal Prediction for Non-Stationary Data

Financial time series are non-stationary, violating the exchangeability assumption. To address this, we employ an adaptive variant that maintains a rolling window of the most recent residuals. Let \mathcal{W}_t be a window of the last W residuals at time t . The adaptive quantile $q_{1-\alpha}(t)$ is the $(1 - \alpha)$ -quantile of \mathcal{W}_t . The prediction interval becomes

$$C_t(X_{\text{test}}) = [\hat{y}(X_{\text{test}}) - q_{1-\alpha}(t), \hat{y}(X_{\text{test}}) + q_{1-\alpha}(t)]. \quad (17)$$

While this no longer provides a strict finite-sample guarantee, it adapts to changes in the error distribution and works well in practice (Gibbs & Candès, 2021).

A.7.3 Portfolio Optimization with Conformal Intervals

The prediction intervals can be used for risk-aware portfolio construction. Consider a portfolio of P assets with weights $\mathbf{w} \in \mathbb{R}^P$ satisfying $\sum_{p=1}^P w_p = 1$ and $w_p \geq 0$. For each asset, we have a point prediction \hat{y}_p and a conformal interval $[\hat{y}_p - q_p, \hat{y}_p + q_p]$. The continuous Kelly criterion maximizes the expected logarithmic growth rate:

$$\max_{\mathbf{w}} \mathbb{E}[\log(1 + \mathbf{w}^\top \mathbf{R})], \quad (18)$$

where \mathbf{R} is the vector of returns. Using a quadratic approximation and the conformal intervals, we approximate

$$\mathbb{E}[\log(1 + \mathbf{w}^\top \mathbf{R})] \approx \mathbf{w}^\top \hat{\mathbf{y}} - \frac{1}{2} \mathbf{w}^\top \hat{\mathbf{\Sigma}} \mathbf{w}, \quad (19)$$

where $\hat{\mathbf{\Sigma}}$ is estimated from the conformal intervals (e.g., as a diagonal matrix with entries q_p^2). The optimization problem becomes

$$\max_{\mathbf{w}} \mathbf{w}^\top \hat{\mathbf{y}} - \frac{\gamma}{2} \mathbf{w}^\top \hat{\mathbf{\Sigma}} \mathbf{w}, \quad \text{s.t. } \mathbf{1}^\top \mathbf{w} = 1, \mathbf{w} \geq 0, \quad (20)$$

with γ a risk aversion parameter. This convex quadratic program can be solved efficiently using differentiable convex optimization layers (Agrawal et al., 2019), enabling end-to-end training.

A.8 Total Loss and Training

The overall loss function combines all components:

$$\mathcal{L}_{\text{total}} = \mathcal{L}_{\text{forecast}} + \lambda_1 \mathcal{L}_{\text{PDE}} + \lambda_2 \mathcal{L}_{\text{MPR}} + \lambda_3 \mathcal{L}_{\text{consist}} + \lambda_4 \mathcal{L}_{\text{symb}}. \quad (21)$$

The hyperparameters $\lambda_1, \dots, \lambda_4$ balance the different objectives. Training proceeds by stochastic gradient descent. Gradients through the SDE solver are computed using the reparameterization trick: the Euler-Maruyama steps are deterministic functions of the initial state and the noise variables $\{\epsilon_j\}$, which are sampled independently of the parameters. Thus, we can backpropagate through the unrolled simulation using automatic differentiation.